Institute of Visualization and Interactive Systems
University of Stuttgart
Universitätsstraße 38
D–70569 Stuttgart

Diplomarbeit Nr. 2956

Discontinuous Galerkin Methods for Two-phase Flows in Porous Media

Christoph Grüninger

Course of Study:	Computer Science (Informatik)
Examiner:	Prof. Dr. Thomas Ertl
Supervisor:	Prof. Dr. Peter Bastian*
	Prof. Dr. Alexandre Ern*
Commenced:	September 1, 2009
Completed:	March 3, 2010
CR-Classification:	G.1.8, G.4, J.2

*Interdisziplinäres Zentrum für Wissenschaftliches Rechnen, Universität Heidelberg

*Centre d'Enseignement et de Recherche en Mathématiques et Calcul Scientifique, École des Ponts ParisTech

Die Mathematiker sind eine Art Franzosen: Redet man zu ihnen, so übersetzen sie es in ihre Sprache, und dann ist es alsbald etwas anderes.

(Johann Wolfgang von Goethe – Maximen und Reflexionen)

Abstract

In this work two-phase flows in porous media are simulated numerically with Discontinuous Galerkin methods. The three methods Symmetrical Interior Penalty Galerkin method (SIPG), Non-symmetrical Interior Penalty Galerkin method (NIPG) and the scheme from Oden, Babuška and Baumann (OBB) are considered. The terminology and the examples are taken from soil science. First the Richards equation is solved using these methods. Then a two-phase flows problem in the saturation/pressure formation is solved with OBB and NIPG. The numerical methods are implemented using the software toolkit PDELab. They are tested with examples from other publications. Weighted averages for absolute and relative permeabilities are examined.

Zusammenfassung

In dieser Arbeit werden Zweiphasen-Strömungen in porösen Medien mit diskontinuierlichen Galerkin-Verfahren numerisch simuliert. Die drei Verfahren Symmetrical-Interior-Penalty-Galerkin-Verfahren (SIPG), Non-symmetrical-Interior-Penalty-Galerkin Verfahren (NIPG) und das Schema nach Oden, Babuška und Baumann (OBB) werden betrachtet. Terminologie und Beispiele stammen aus der Bodenkunde. Zuerst wird die Richards-Gleichung mit den genannten Verfahren gelöst. Danach wird ein Strömungsproblem mit zwei Phasen in der Druck/Sättigungs-Formulierung mit OBB und NIPG gelöst. Die numerischen Verfahren sind mit Hilfe des Software-Toolkits PDELab implementiert. Sie werden anhand von Literaturbeispielen getestet. Gewichtete Mittel (weighted averages) werden für absolute und relative Permeabilitäten untersucht.

Résumé

Dans ce travail des écoulements diphasiques en milieu poreux sont simulés avec les méthodes Galerkine discontinues. Trois méthodes sont considérées: la méthode Symmetrical Interior Penalty Galerkin (SIPG), la méthode Non-symmetrical Interior Penalty Galerkin (NIPG) et le schéma d'Oden, Babuška et Baumann (OBB). La terminologie et les exemples sont dû à la pédologie. Tout d'abord l'équation de Richards est résolue avec les méthodes ci-dessus. Ensuite un problème d'écoulements diphasiques à la formulation de pression/saturation est résolu avec OBB et NIPG. Les méthodes numériques sont implémentées avec le logiciel PDELab. Elles sont testés avec des exemples qui sont dû à autres publications. Les moyennes pondérées (weighted averages) pour des perméabilités absolues et relatives sont étudiées.

Contents

1 Introduction

1.1 Motivation

Water is the source of life on Earth. No species is known to survive permanently in the absence of water. Humans for example consume about 800 km^3 of drinking water per year. Considering that only 20 % of this demand is met by fresh water from the surface of the Earth, groundwater reserves play an important role as water supplies not only in arid environments. One quarter of the pumped groundwater is taken from fossil groundwater reserves. With groundwater supplies being non-renewable and prone to pollution it is essential to protect these resources and use them wisely.

All over the world industry and modern agriculture endanger the groundwater by their pollution. Oil, sewage, fertilizers, drugs and other chemicals are handled in large quantities and are able to enter the soil by accident or carelessness. Once polluted, only small areas of soil can be cleaned with costly procedures. [Bas1999] cites a source from 1996 which estimates the cleanup costs for all contaminated sides in Germany to a total of 50 to 150 billion euros.

In the last 50 years commercial nuclear energy has been used and caused additional pollutions. The used nuclear fission leaves radioactive waste, which can cause cancer or even death. The biosphere must be protected from this waste for up to thousands of years. Even though the dangers of nuclear waste are known, no long-term solution has been found. Scientists all over the world research the possibilities of underground storage facilities. In the 1970s Germany stored 250 m^3 medium-level waste in the old Asse 2 mine. The waste is kept 511 m below the subsurface in a former rock-salt mine. According to [Sch2009] it is still not clear whether nuclear contaminated water can reach the surface before its radioactivity decays to a safe level.

Knowledge of water movement can both improve the exploitation of limited reserves and protect as much water as possible for future usage. The mechanisms of groundwater movement must be known to properly specify water protection areas and anticipate potential dangers arising from pollutions. Soil science examines these problems with mathematical models. In many cases two phases are considered. E.g. groundwater and soil air or petroleum and water are often modeled this way.

In general the two models used in this work cannot be solved analytically. Numerical methods can find approximated solutions but the methods contain many difficulties. Amongst others the difficulties are non-linear functions, discontinuities, singularities, complicated

meshes with the need for local refinement, large systems of linear equations, heavy memory consumption and complicated softwares that have been growing over time. Different approaches must be tried to find the feasible ones which can be used for applications. Supported by theoretical considerations and experiences from other fields an almost new way is tried in the present work.

1.2 Scientific Computing

The term scientific computing evolved throughout the last years. It does not define a new discipline, it rather is a joined effort of researchers with different backgrounds. Scientific computing is the overlapping area of mathematics, computer science, physics with applications in geology, biology, engineering, astronomy and soil science.

Computer simulations are a major tool for soil science, see [KBS+2003]. Similar problems in other disciplines have helped to implement simulations meeting the specific needs and difficulties of soil science simulations.

The starting point for a simulation is an informal description of the conceptual model. It contains all necessary physical effects which are taken into consideration. Simplifications and additional assumptions must be justified in the context of the applied discipline.

A mathematical model must be evolved from the conceptual model. It describes all physical laws in a quantitative manner. Usually the mathematical model contains systems of partial differential equations (PDE) which may be time-dependent, coupled and non-linear. Questions in this part of scientific computing are the existence of solutions and their uniqueness.

In general the mathematical model cannot be solved directly. A discrete numerical model that can be solved by computers must be found. To reach the desired accuracy, huge systems of linear or non-linear equations are necessary. In numerical analysis the convergence speed of algorithms is crucial, because of the large amounts of input data.

The resulting computer programs are complex and flexible enough to solve various simulations. Nevertheless the program must be as fast as possible. Computer scientists work on optimizing compilers, parallelization, hardware respecting code and modularization as key methods to achieve the contradictory goals. Especially concurrently running code is error prone but the only way to tap the full potential of modern massively parallel supercomputers.

The simulation results are compared to measured data. To match the desired accuracy the modelling process must be repeated and improved multiple times. One has to keep the whole process and its weak points in mind. It is useless to improve the accuracy in one part when an other part dominate the error.

Single pieces of the modelling process can be improved seperately. In large simulations difficult areas are identified and test problems are extraced and published.

1.3 About this work

The objective of this work is to write fast simulation programs with today's mathematical methods and an existing software toolkit. The interdisciplinary components mentioned in the last section, such as the conceptual or the mathematical model, are also being discussed because they form the basic principles for the implemented numerical model. To understand their numerical models a profound knowledge is required.

Simulations of subsurface water movement use different numerical approches. Discontinuous Galerkin (DG) methods are successfully used in many fields, but are rarely adopted for the two-phase flows in the pressure/saturation formulation. With a program practical experience is collected and the different formulations can be compared numerically. The DG methods used in this work are Symmetrical Interior Penalty Galerkin method (SIPG), Non-symmetrical Interior Penalty Galerkin method (NIPG) and the scheme from Oden, Babuška and Baumann (OBB). The time is discretized with the Crank-Nicolson or the implicit Euler scheme.

To become more acquainted with parabolic PDEs and to get a feeling for groundwater flows the Richards equation is implemented. The model assumes a constant soil air pressure. This leaves only one independent variable which reduces the efford to implement a solver. The results of [Soc2008] are reproduced.

As a second step a two-phase flows solver are implemented, using the uncommon pressure/saturation formulation from [Eps2007]. Finally the results are compared to other formulations or other discretization methods.

In Chapter 2 the relevant physical effects are described. The mathematical model is presented in the following chapter. Chapter 4 describes the used software toolkit. Chapters 5 and 6 present numerical results for the Richards equation and general two-phase flows in porous media. The last chapter contains this work's conclusions.

2 Flows in porous media

This chapter introduces the terminology and the models used in simulations of fluids in porous media. First porous media are defined and relevant effects occurring in reality are described. Later a mathematical model for two-phase flows is given.

Brief introductions of flows in porous media are included in [KL2000] and [Hol1996]. [Bas1999] presents a deeper but still compact overview.

2.1 Terminology

A porous medium is a heterogeneous body which consists of a solid part with small enclosed pores. The solid part is called solid matrix and the other part's name is pore space or void space. The pores are connected with each other and are filled with one or more fluids which are able to move through the pores, see figure 2.1.

The fluids can be liquids or gases. Locally on the scale of a pore they form phases which means that small fluid portions are chemically homogeneous and separated from other portions of different fluids by a definite physical boundary. A multiphase system or k-phase system contains k different phases which are not miscible. Liquids can be miscible e.g. fresh water and salt water or water and alcohol, which form a solution. Then again they can also be immiscible like water and oil. Gases only form one phase because they are always miscible. Sometimes the solid matrix is considered as an additional phase, called solid phase, which leads to a k+1-phase system.

Flows through porous media occur in a variety of applications. Blood flows in a human brain, groundwater flows, gases in foamed ceramics or porous catalytic converters are examples

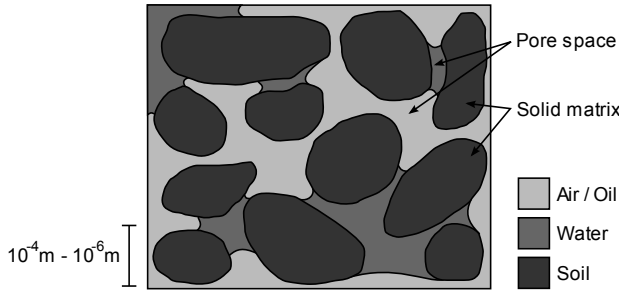

Figure 2.1: Two non-miscible fluids in a porous medium

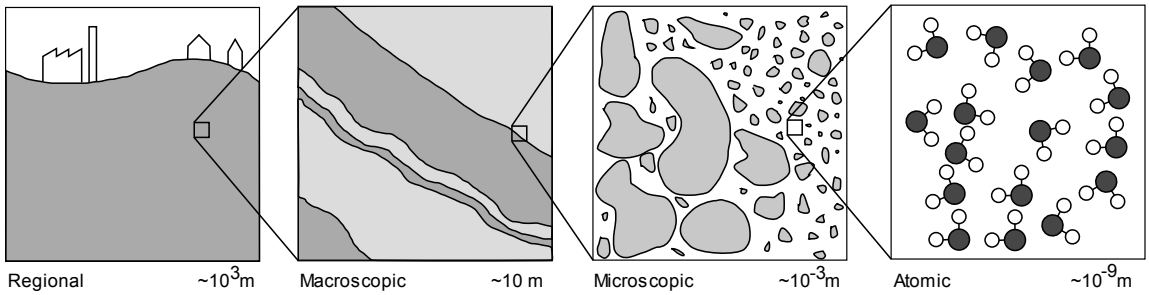

Figure 2.2: Subsurface length scales, after [Bas1999]

of one-phase flows. In petroleum geology the two-phase problem of water and oil flows in soil is studied to identify oil reservoirs for exploitation. In soil science groundwater and subsurface air are the fluids being historically studied e.g. in [Ric1931]. Three-phase flows in porous media occur in the field environmental protection where oil polluted soil containing water and air is studied. In this paper only two-phase flows will be studied. The focus is on soil science problems: its terminology is used and the examples are taken from this area.

2.1.1 Length scales

Different scales occur in soil science as schematically drawn in Figure 2.2. On a regional perspective (~10^3 m) water sources and sinks, large geological structures, the effects of pollution and groundwater extraction are considered. Stacked material layers, foldings, faults and cracks are looked at on a macroscopic scale (~10 m). In microscopic areas (~10^{-3} m) curls, drags and capillary pressure occur in the complicated shaped pores. On the lowest level (~10^{-9} m) atoms interact and react. All chemical processes happen there.

The scale of atoms or soil pores is not useful for models describing field-scale processes, lab experiments and even less for catchment areas or underground waste sites. One liter of water contains about 10^{25} molecules. To avoid this complexity the continuum approach is used. A hypothetical continuum on the macroscopic scale is used instead of discrete molecules. Mass, density or pressure are considered continuous quantities. This approach must be justified by physical properties which are fulfilled in our case.

2.1.2 Porosity

Porosity ϕ is the fraction of a given volume which is not occupied by soil. If there are no pores at all, the porosity ϕ is 0. If no soil is in the volume, ϕ is 1. The definition of porosity at a single point would be senseless. It would be the characteristic function for void space

$$\chi_{void}(x) = \begin{cases} 0 & x \in \text{solid matrix} \\ 1 & x \in \text{pore space} \end{cases} \tag{2.1}$$

for all $x \in \Omega$ where the domain $\Omega \subset \mathbb{R}^d$ is the area of interest.

Let the volume V be chosen suitably and x be the center of V. Then the porosity is defined via

$$\phi(x) = \frac{\int_V \chi_{void}(\xi)\,\mathrm{d}\xi}{\int_V 1\,\mathrm{d}\xi}. \tag{2.2}$$

2.1.3 Saturation

When the pore space is completely filled with water it is called saturated. In soil this is the case below the groundwater table. Above this level in the so called unsaturated zone both water and air reside in the pores.

Saturation S indicates the proportionate content of the pore space. If a phase α fills the pores completely, its saturation is $S = 1$. If the phase is not present, it is $S = 0$. A characteristic function for the α-phase is similar to the one given above.

$$\chi_\alpha(x) = \begin{cases} 0 & x \notin \text{phase } \alpha \\ 1 & else \end{cases} \tag{2.3}$$

Like porosity saturation is only defined with the aid of a suitable volume V:

$$S_\alpha(x) = \frac{\int_V \chi_\alpha(\xi)\,\mathrm{d}\xi}{\int_V \chi_{void}(\xi)\,\mathrm{d}\xi} = \frac{\int_V \chi_\alpha(\xi)\,\mathrm{d}\xi}{\phi(x)\int_V 1\,\mathrm{d}\xi}. \tag{2.4}$$

In a two-phase system the pore space must be filled with either of the phases

$$S_\alpha + S_\beta = 1. \tag{2.5}$$

A phase cannot vanish completely from soil. In pockets and small pores portions of the phase remain and are stuck in their place. Only vaporization or a changing solid matrix would demobilize them, but both mechanisms are beyond the scope of this work. The α-phase residual saturation $S_{\alpha r}$ gives α's minimal saturation which is usually greater than zero. It is a property of the porous medium and the phase.

The effective saturation

$$\bar{S}_\alpha = \frac{S_\alpha - S_{\alpha r}}{1 - \sum_\beta S_{\beta r}} \tag{2.6}$$

for all phases β, describes the saturation concerning the remaining pore space which is not filled by residual parts of the phases. This value is used to formulate physical laws in soil.

2.1.4 Density and gravitational acceleration

The density ρ is a property of the phase. It is the mass per volume and is measured in $^{kg}/_{m^3}$.

Gases and to a smaller extent fluids are compressible, thus their density depends on pressure. The examples in this work have constant densities but the compressible character of the phases is kept in mind.

Near the surface everything is accelerated towards the Earth's core with a rate between $9.75\,^{m}/_{s^2}$ and $9.83\,^{m}/_{s^2}$. This location dependent value is called gravitational acceleration g. It is a vector with the z-coordinate pointing downwards, e.g.

$$g = \begin{pmatrix} 0 \\ 0 \\ -9.81 \end{pmatrix}.$$

Nota bene, in this work equations may be divided by $\rho\, g$ while retaining all symbols.

2.1.5 Pressure and pressure head

The pressure p in $\mathrm{Pa} = {}^{kg}/_{m\cdot s^2}$ increases with growing depth from the surface. Without any water-movement, in the hydrostatic case, the linear law

$$p = -\rho\, g\, z \tag{2.7}$$

is valid. The depth z in m is zero at the groundwater table where the saturated groundwater ends and the unsaturated zone begins. In the saturated zone z is negative and becomes positive in the direction to the surface. Some books define z the other way round.

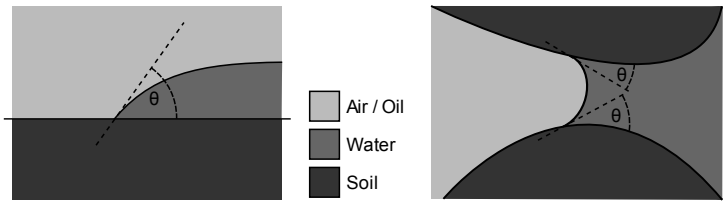

Figure 2.3: Surface tension between the wetting phase water and the non-wetting phase air or oil with contact angle θ, after [Hol1996]

A pressure value can be linked to the depth which would impose the same pressure. It is called pressure head and can be calculated in the hydrostatic case by $\frac{p}{\rho g}$. It is measured in m and will be used in this work synonymously.

The pressure must differ from the hydrostatic case for groundwater flows. The difference is called hydraulic pressure $p + \rho g z$. The piezometric head

$$h = \frac{p}{\rho g} + z \tag{2.8}$$

is the same value, interpreted as a depth in m. It can be measured with a piezometer, a small-diameter vertical tube. The relative pressure compared to the pressure head is measured on its tip.

2.1.6 Capillary pressure

If a porous medium contains more than one fluid, they are distinguished as wetting phase and non-wetting phase. For every pair of fluids one is the wetting and the other is the non-wetting phase. It is a physical property of both fluids which fluid is wetting. A gaseous phase is always non-wetting. Water is the wetting phase if the second one is oil. From now on the fluids are only called wetting and non-wetting phase. The subscripts w and n label variables for the wetting and the non-wetting phase. If something applies similar for both phases the subscript $\alpha \in \{w, n\}$ is used.

On the boundary surface between two fluids a pressure difference occurs and is called capillary pressure p_c. It results from different inter-molecular forces which sum up to zero inside the phase but are different from zero on the boundary surface because of the different forces from the other phase. The pressure difference bends the boundary surface by a fluid-specific contact angle θ. Figure 2.3 shows two cases where θ occurs. Per definition the wetting phase has a wetting angle $\theta < 90°$.

The capillary pressure on the pore level would be to difficult to simulate. It is replaced by a macroscopic pressure difference

$$p_c = p_n - p_w \tag{2.9}$$

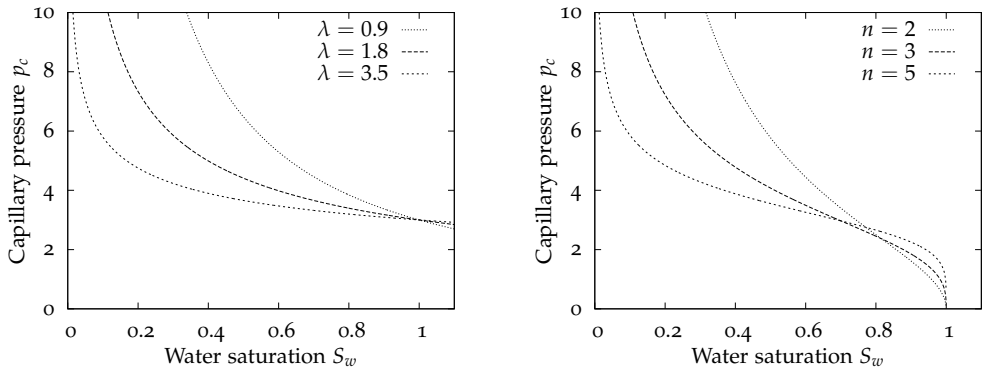

Figure 2.4: Capillary pressure models from (a) Brooks-Corey with $p_e = 3$ and (b) van Genuchten with $\alpha = 0.3$

which is always positive. It was identified in experiments that p_c can be described by non-linear functions depending on the effective saturation $\bar{S}_w$. The functions were developed with theoretical considerations in mind and fitted to measured data. There exist various models for capillary pressure. In the following two models named after their inventors are presented.

The Brooks-Corey model

$$p_c(S_w) = p_e \, \bar{S}_w^{-\frac{1}{\lambda}} \tag{2.10}$$

has two parameters. The entry pressure p_e is the pressure needed for the wetting phase to enter large pores which are completely filled with the non-wetting phase. The pore size distribution λ is high if the soil is made from same sized grains. With different sized grains it becomes smaller. Its range in natural soils is between 0.2 and 3.0. Figure 2.4a shows some graphs with changing λ. This model was first published in 1964.

The model from van Genuchten [vG1980] adopted for two-phase systems describes the capillary pressure

$$p_c(S_w) = \frac{1}{\alpha} \left(\bar{S}_w^{-\frac{1}{m}} - 1 \right)^{\frac{1}{n}} \tag{2.11}$$

with α, m and n as parameters. Typical $m = 1 - \frac{1}{n}$ is chosen. The reciprocal of parameter α is analog to the entry pressure p_e in the Brooks-Corey model. In most cases n lies within the interval from 2 to 5. In figure 2.4b some examples with different n are given.

In reality a hysteresis effect occurs. If the saturation increases the capillary pressure is higher compared to the value for decreasing saturation. The simplified models can be used if the effective saturation does not oscillate between its extreme values.

Both models show the core problem of numerical simulations of two-phase flows. The capillary pressure may become very large and steep for small effective saturations $\bar{S}_w$. This reduces the numerical accuracy and increases the necessary steps with the Newton solver. One has to bear in mind that the model functions are not defined for effective saturations below 0 or above 1.

2.1.7 Mobility and Permeability

The mobility

$$\lambda_\alpha(S_\alpha) = \frac{k_{r\alpha}(S_\alpha)}{\mu_\alpha} \tag{2.12}$$

is a combination of properties from the fluid and the solid matrix.

The dynamic viscosity μ_α describes friction inside the fluid. A faster flowing fluid has a smaller viscosity, it is measured in $^{\mathrm{kg}}/_{\mathrm{m\cdot s}}$ or $\mathrm{Pa}\cdot\mathrm{s}$.

The relative permeability $k_{r\alpha}(S_\alpha)$ is dimensionless and stays in the range from 0 to 1. The flow of a phase is interfered by the other phase which thus influences the permeability. If the wetting phase vanishes, the non-wetting is not blocked and k_{rw} is 1. The wetting phase is blocked completely if the wetting phase fills the pores completely, k_{rw} is 0. The same applies vice versa.

The capillary pressure p_c is closely linked with the relative permeability. Many parameters are adjusted to the parameters of the capillary pressure. Matching to the models above, two models for the relative permeability are presented.

The Brooks-Corey model

$$k_{rw}(S_w) = \bar{S}_w^{\frac{2+3\lambda}{\lambda}} \tag{2.13a}$$

$$k_{rn}(S_n) = \bar{S}_n^2 \left(1 - (1 - \bar{S}_n)^{\frac{2+\lambda}{\lambda}}\right) \tag{2.13b}$$

shares λ with the capillary pressure, and is shown exemplarily in Figure 2.5a.

The model from van Genuchten

$$k_{rw}(S_w) = \bar{S}_w^{\varepsilon} \left(1 - \left(1 - \bar{S}_w^{\frac{n}{n-1}}\right)^{\frac{n-1}{n}}\right)^2 \tag{2.14a}$$

$$k_{rn}(S_n) = \bar{S}_n^{\gamma} \left(1 - (1 - \bar{S}_n)^{\frac{n}{n-1}}\right)^{\frac{2(n-1)}{n}} \tag{2.14b}$$

has additional parameters ε and γ. They can be set to $\varepsilon = \frac{1}{2}$ and $\gamma = \frac{1}{3}$. The suggested choice for $m = 1 - \frac{1}{n}$ is already included. Figure 2.5b contains graphs for two different values for n.

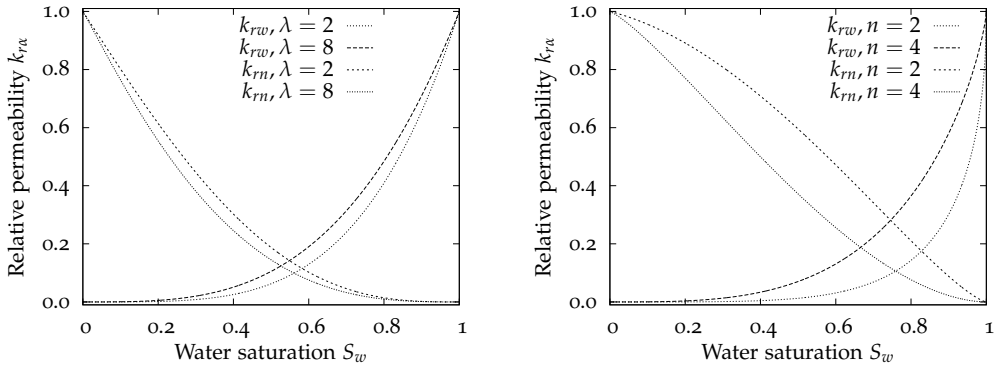

Figure 2.5: Capillary pressure models from (a) Brooks-Corey and (b) van Genuchten with $\varepsilon = \frac{1}{2}$ and $\gamma = \frac{1}{3}$

Soil	Absolute permeability in m^2
Gravel	$> 10^{-9}$
Coarse sand	10^{-11} to 10^{-10}
Fine sand	10^{-13} to 10^{-11}
Clay	$< 10^{-17}$

Figure 2.6: Absolute permeabilities for some soils, [Hol1996]

The absolute permeability K is a macroscopic simplification of the soil's macroscopic structure. Different grain sizes, grain shapes and their arrangement on the microscopic scale are averaged. It is location dependent, anisotropic and its discontinuities can exceed several orders of magnitude as shown in Figure 2.6. The absolute permeability is measured in m^2 and is a positive symmetric tensor.

2.1.8 Darcy velocity

The velocities of the fluids on the microscopic scale differ locally. In the middle of a pore the velocity is higher compared to the borders where friction slows the fluids down. Curls and reverse flows may occur depending on the pore geometry. In general the pore space is not known in such detail.

As already used for porosity and saturation a suitable volume V is used. With total discharge Q, which passes a cross-sectional area A of V, the Darcy velocity

$$u = \frac{Q}{A} \tag{2.15}$$

is defined. Its unit is $^{m}/_{s}$. Q and A can be measured and v is a continuous value. For a multi-phase system a velocity per phase can be defined.

2.1.9 Sources and sinks

Various hydraulical, physical, chemical or biological processes can emit or consume mass of a phase. The source or sink q is positive if mass is added. It is measured in $^{kg}/_{m^3 \cdot s}$. In most test cases is $q = 0$.

2.2 Two-phase flows in porous media

With the terminology from the last section the analytic description of two-phase flows and the reduced Richards equation can be introduced.

2.2.1 Conservation law

The conservation of mass

$$\frac{\partial}{\partial t}(\phi S \rho) + \nabla \cdot (\rho u) = q \tag{2.16}$$

is the basis of the analytic description of flows. In the integral form the equation states that the mass in a volume V and the flows over the borders ∂V are equal to productions or reductions inside of V. This law can be obtained from a specialization of Reynolds transport theorem.

2.2.2 Darcy's law

The one-dimensional case was experimentally found by Henry Darcy in 1856. In today's form it is

$$u_\alpha = -\frac{k_{r\alpha}(S_\alpha)}{\mu_\alpha} K (\nabla p_\alpha - \rho_\alpha g) = -\lambda_\alpha(S_\alpha) K (\nabla p_\alpha - \rho_\alpha g). \tag{2.17}$$

Darcy's law is a special case of the Navier–Stokes equation and can be regarded as a momentum conservation law.

The equation is only valid for laminar flows which means the absence of turbulences and low flow velocities. It is false for steep pressure gradients and fissured soils like karst.

2.2.3 Two-phase flows problem

With the substitution of u in (2.16) by (2.17) the analytical problem description of the two-phase flows has 4 unknowns: 2 saturations S_w and S_n, 2 pressures p_w and p_n. Together with the sum of saturations (2.5) and capillary pressure (2.9) the problem is specified by the 4 equations in $\Omega \subset \mathbb{R}^3$:

$$S_w + S_n = 1 \tag{2.18a}$$

$$p_c(S_w) = p_n - p_w \tag{2.18b}$$

$$\frac{\partial}{\partial t}\left(\Phi \rho_\alpha S_\alpha\right) - \nabla \cdot \left(\rho_\alpha \lambda_\alpha(S_\alpha) K \left(\nabla p_\alpha - \rho_\alpha g\right)\right) = q_\alpha \qquad \text{for } \alpha \in \{w, n\} \tag{2.18c}$$

with initial conditions

$$S_\alpha(x, 0) = S_{\alpha_0}(x) \qquad p_\alpha(x, 0) = p_{\alpha_0}(x) \qquad \text{for } \alpha \in \{w, n\} \tag{2.18d}$$

and boundary conditions

$$S_\alpha(x, t) = g_{S_\alpha}(x, t) \qquad p_\alpha(x, t) = g_{p_\alpha}(x, t) \qquad \text{on } \partial\Omega_{D,\alpha} \text{ for } \alpha \in \{w, n\} \tag{2.18e}$$

$$\rho_\alpha \lambda_\alpha(S_\alpha) K \left(\nabla p_\alpha - \rho_\alpha g\right) = j_\alpha(x, t) \qquad \text{on } \partial\Omega_{N,\alpha} \text{ for } \alpha \in \{w, n\} \tag{2.18f}$$

These equations can now be combined in various ways. Always two non-linear coupled equations with two independent unknowns must be solved. According to the unknowns the initial and boundary conditions must be given. Some choices and their advantages are discussed in the following.

2.2.4 Pressure/saturation formulation

The first formulation has the unknowns S_n and p_w. (2.18a) and (2.18b) replace S_w and p_n.

$$\frac{\partial}{\partial t}\left(\Phi \rho_w \left(1 - S_n\right)\right) - \nabla \cdot \left(\rho_w \lambda_w (1 - S_n) K \left(\nabla p_w - \rho_w g\right)\right) = q_w \tag{2.19a}$$

$$\frac{\partial}{\partial t}\left(\Phi \rho_n S_n\right) - \nabla \cdot \left(\rho_n \lambda_n(S_n) K \left(\nabla p_w + \nabla p_c(1 - S_n) - \rho_n g\right)\right) = q_n \tag{2.19b}$$

In this formulation S_n and S_w can be interchanged with (2.18a) and it does not affect any property of the system. The independent variables easily be changed to p_n and S_w by redefining k_{rw}, k_{rn} and p_c. The choice between p_w and p_n to be an unknown must ensure that the saturation of the chosen pressure does not vanish. The partial pressure of a non-existing phase is undefined.

2.2.5 Elliptic pressure/saturation formulation

Adding the equations (2.18c) for both phases, together with the supplementary assumption of incompressible phases and equation (2.18a), causes the storage term to vanish. The wetting phase equation is the same as in the last formulation. The system has an elliptic equation and a parabolic one.

$$\begin{aligned} -\nabla \cdot \big(\rho_w \lambda_n (1-S_n) K (\nabla p_w - \rho_w g) + \rho_n \lambda (1-S_n) K \big(\nabla p_w + \nabla p_c (1-S_n) - \rho_n g\big)\big) \\ = q_w + q_n \end{aligned} \tag{2.20a}$$

$$\frac{\partial}{\partial t}\left(\Phi \rho_w (1-S_n)\right) - \nabla \cdot \left(\rho_w \lambda_w (1-S_n) K (\nabla p_w - \rho_w g)\right) = q_w \tag{2.20b}$$

The elliptic equation is easier to solve compared to the last formulation. But the limitation to incompressible flows disqualifies this formulation for further examination in this work.

2.2.6 Global pressure formulation

A new variable called global pressure p can be defined by

$$p(x,t) = p_n(x,t) + p_c(1-S_{nr}) - \int_{1-S_{nr}}^{1-S_n(x,t)} \frac{\lambda_w(\xi)}{\lambda_w(\xi)+\lambda_n(\xi)}\, p_c{}'(\xi)\, \mathrm{d}\xi \tag{2.21}$$

with S_{nr} the residual saturation of the wetting phase.

Analog to the pressure/pressure formulation with incompressible flows this leads to

$$-\nabla \cdot \left(\rho_w \lambda_w (1-S_n) K (\nabla p - \rho_w g) + \rho_n \lambda_n (1-S_n) K (\nabla p - \rho_n g)\right) = q_w + q_n \tag{2.22a}$$

$$\frac{\partial}{\partial t}\left(\Phi \rho_w (1-S_n)\right) - \nabla \cdot \left(\rho_w \lambda_w (1-S_n) K (\nabla p_w - \rho_w g) - \lambda_h K \nabla p_c (1-S_n)\right) = q_w \tag{2.22b}$$

with $\lambda_h = \dfrac{\rho_w \lambda_w (1-S_n) + \rho_n \lambda_n (1-S_n)}{\rho_w \lambda_w (1-S_n) \rho_n \lambda_n (1-S_n)}$ and the independent variables S_n and p_w.

This formulation needs more extensive assumptions. The phases must be incompressible, the fractional flow $f_w := \frac{\lambda_w}{\lambda_w + \lambda_n}$ and the capillary pressure p_c must depend only on the saturation S_w.

The global pressure is an artifical value. Thus it cannot be measured experimentally and boundary conditions for simulations must be calculated. But the formulation leads to less steep pressure gradients, it is allways well defined and handy for theoretical proofs.

[Bas1999] explains the backgrounds of this formulation in more detail. The global pressure formulation is not used in this work.

2.2.7 Pressure/pressure formulation

If the inverse function of the capillary pressure is known, the saturation can be calculated from both phase pressures:

$$S_w = p_c^{-1}(p_n - p_w) \tag{2.23}$$

With this function and (2.18a) the independent variables can be p_n and p_w.

$$\frac{\partial}{\partial t}\left(\Phi\rho_w\, p_c^{-1}(p_n - p_w)\right) - \nabla\cdot\left(\rho_w\lambda_w\left(p_c^{-1}(p_n - p_w)\right) K\left(\nabla p_w - \rho_w g\right)\right) = q_w \tag{2.24a}$$

$$\frac{\partial}{\partial t}\left(\Phi\rho_n\left(1 - p_c^{-1}(p_n - p_w)\right)\right) - \nabla\cdot\left(\rho_n\lambda_n\left(p_c^{-1}(p_n - p_w)\right) K\left(\nabla p_n - \rho_n g\right)\right) = q_n \tag{2.24b}$$

This formulation does not need additional assumptions. This formulation is not further considered.

2.3 The Richards equation

In some cases with water and air in the unsaturated zone one can assume a constant air pressure. When the soil air is connected to the air above the ground, and water percolates slow enough for air bubbles to escape upwards, soil air has atmospheric pressure. By scaling the atmospheric pressure to $p_n = 0$, the water pressure becomes $p_w = -p_c$. With the incompressibility of water, i.e. the density ρ_w is constant, and a saturation function $S(p_w) := p_c^{-1}(-p_w)$ the problem simplifies to the equation

$$\frac{\partial}{\partial t}S(p_w) - \nabla\cdot\left(K(p_w)\left(\nabla p_w - z\right)\right) = q_w \qquad \text{in } \Omega\times[0,T], \tag{2.25a}$$

$$p_w = g \qquad \text{on } \partial\Omega_D\times[0,T], \tag{2.25b}$$

$$-(K(p_w)\nabla p_w)\cdot\nu = j \qquad \text{on } \partial\Omega_N\times[0,T], \tag{2.25c}$$

$$p_w(\cdot,0) = p_0 \qquad \text{in } \Omega\times 0. \tag{2.25d}$$

Both S and K are monotone non-linear functions. The relative and absolute permeability are contained in K which depends on p_w and may depend on the position x. This equation is a non-linear form of the parabolic heat equation and was first published in [Ric1931].

The water pressure is $p_w = 0$ at the groundwater table. Beneath the saturated zone the water pressure is positive, above in the unsaturated zone negative. For many saturation functions $\frac{\partial}{\partial t}S(0) = 0$ holds and the equation reduces to an elliptic problem. With $S(p_w) := 1$ and $K(p_w) := K(0)$ for $p_w > 0$ the Richards equation can be extended to include the saturated zone.

3 Discretization

In general the analytical models for two-phase flows in porous media mentioned in the previous chapter cannot be solved analytically. Numerical methods are tried and tested, theoretical results like error estimates back this approach up in many cases.

The object of this work is to develop a discontinuous Galerkin method. This chapter requires knowledge about Galerkin methods and especially about standard finite element methods (FEM). For this topic [Bra2007] may serve as an in-depth source.

The disretization is a reduction of the infinite function space, which contains the solution, to a finite function space. In the finite function space the solution can be approximated.

The parabolic equations are defined on $[0, T] \times \Omega$. The method of lines indicates to discretize time $[0, T]$ and space Ω separately. Both are continuous and can be approximated by a discrete representation. Figure 3.1 shows the sequence of elliptic problems after a time discretization.

3.1 Time discretization

Time is sliced in time steps of finite length. The points of time are consecutively named $t_i,\ i \in \{0, 1, 2, \dots\}$. In general the distance between two points of time may vary. In this work every time step has the same length $\Delta t = t_{i+1} - t_i$.

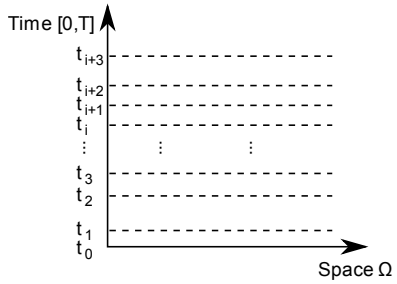

Figure 3.1: Discretization with the method of lines. Every dotted line is an elliptic problem to be solved for a discrete point of time, a system of ordinary differential equations occurs between two points of time

3.1.1 Ordinary differential equations

A simple example for a parabolic problem is

$$\frac{\partial}{\partial t}u(x,t) - \Delta u(x,t) = 0 \tag{3.1}$$

which is used to show the time discretization. The results can be applied to the model problems from the last chapter. The first term is differentiated with respect to t, the second twice with respect to x. Be $\Omega(h(t))$ a discretization of the elliptic part $-\Delta u(x,t) = 0$ on a grid $h(t)$ as described in the next section. Then holds

$$\frac{\partial}{\partial t}h(t) = \Omega(h(t)) \tag{3.2}$$

which is an ordinary differential equation.

In an integral form of (3.2)

$$h(t_{i+1}) = h(t_i) + \int_{t_i}^{t_{i+1}} \Omega(h(\tau))\,\mathrm{d}\tau \tag{3.3}$$

the right hand side can be approximately solved with numerical integration.

The easiest approach is to use the solution of the old point of time $\Omega(h(t_i))$ and multiply by the step length Δt.

$$h(t_{i+1}) = h(t_i) + \Omega(h(t_i))\,\Delta t \tag{3.4}$$

The resulting time discretization is called forward or explicit Euler method. This method is conditionally stable. The explicit Euler method has to satisfy a ratio between time step Δt and width of space discretization h for convergence. This limitation lowers the practical use for the examined equations because the time step becomes very small especially for fine space discretizations.

A better way for diffusive equations is to choose the solution at the new point of time t_{i+1} instead.

$$h(t_{i+1}) = h(t_i) + \Omega(h(t_{i+1}))\,\Delta t \tag{3.5}$$

This gives the backward or implicit Euler method, which is a sufficient stable method for the examined equations. But $\Omega(h(t_{i+1}))$ is unknown and a linear or even non-linear system must be solved to determine it. Explicit and implicit Euler methods have an order of convergence of 1. This means that by halving the time step Δt the error halves, too.

A combination of both Euler methods is the θ scheme, a convex combination of the form

$$h(t_{i+1}) = h(t_i) + \Big(\theta\,\Omega(h(t_{i+1})) + (1-\theta)\,\Omega(h(t_i))\Big)\,\Delta t. \tag{3.6}$$

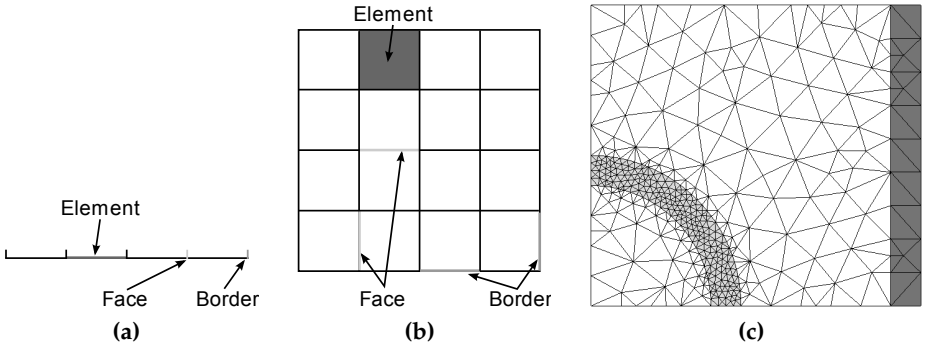

Figure 3.2: Space discretization (a) one-dimensional, (b) two-dimensional with structured rectangles and (c) two-dimensional with triangles from a real world example, [NNa] / [NNb]

Choosing $\theta = 0$ or $\theta = 1$ result in the two Euler methods. It can be shown that $\theta < \frac{1}{2}$ is not stable like the explicit Euler method and $\theta = \frac{1}{2}$ has a convergence rate of 2. This method is referred to as Crank-Nicolson method. Regarded as a numerical quadrature rule the Crank-Nicolson method is the trapezoidal rule.

To achieve even higher convergence rates it is necessary to use more time steps. Additional points of time between $\Omega(h(t_i))$ and $\Omega(h(t_{i+1}))$ lead to Runge–Kutta methods. Multistep methods use older points of time $\Omega(h(t_{i-1})), \Omega(h(t_{i-2})), \ldots$ to improve the convergence rate. Both approaches are less stable than the implicit Euler. In this work only the implicit Euler and the Crank-Nicolson method are used.

3.2 Space discretization

Splitting the domain Ω into smaller pieces is called triangulation. The pieces are called elements, together they form a mesh or grid. In one-dimensional triangulations they are line segments. In two dimensions triangles and rectangles are common and in three dimensions cubes and tetrahedrons are used. In higher dimensions hypercubes and simplices serve as elements. Sometimes other shapes or more than one type of shape are employed. The elements can have different sizes or orientations like in Figure 3.2c or form a structured mesh like in Figure 3.2b. For adaptivity elements can be refined locally as shown in Figure 3.2c near the segment of a circle in the left bottom corner. In this work grids are limited to structured rectangular meshes.

3.2.1 Definitions

The union of all elements $e \subset \Omega$ from the set of elements E cover the whole domain

$$\bigcup_{e \in E} e = \Omega. \tag{3.7}$$

For every pair of elements $e_i \in E$ and $e_j \in E$, $i \neq j$, the intersection $e_i \cap e_j$ is a shape of co-dimension 1 or higher. E.g. for two-dimensional elements the intersection $e_i \cap e_j$ may be a line or a point but not a shape with a positive area. For three-dimensional elements the intersection $e_i \cap e_j$ must have no volume. The shapes of co-dimension 1 are called faces f or intersections and the set of all faces is F. The intersections of higher co-dimensions are insignificant for this work.

Every face $f \in F$ has an arbitrary constant inside and outside element e^- and e^+ with $e^- \cap e^+ = f$. The two normals ν^- and ν^+ exist with regard to f. The outer normal of the inside element ν^- points from the inside to the outside element and ν^+ in the opposite direction, see figure 3.3b. From now on only

$$\nu := \nu^- = -\nu^+ \tag{3.8}$$

will be used. The evaluation of a function u at a face $f \in F$ on the inside element is named $u^-(x) := u(x)\big|_{inside}$, $x \in f$ and analog $u^+(x) := u(x)\big|_{outside}$, $x \in f$.

The intersection of an element $e \in E$ with the domain border $\partial\Omega$ is called border intersection or just border. The sets $F_D := \{e \cap \partial\Omega_D \,|\, e \in E\}$ and $F_N := \{e \cap \partial\Omega_N \,|\, e \in E\}$ contain intersections of the elements and the domain border with Dirichlet or Neumann conditions. The outer normal ν for borders is defined as the normal pointing from the inside element to the outside of Ω.

The numerical solution can be discontinuous on faces. It is necessary to quantify the size of the discontinuity. Let for every $x \in f \in F$ be

$$[u](x) = u^-(x) - u^+(x) \tag{3.9}$$

defined as the jump of function u on face f.

A function u is undefined at a discontinuity on a face. To close this gap in the definition the average u is used. Let for every $x \in f \in F$ be

$$\langle u \rangle(x) = \frac{1}{2}\big(u^-(x) + u^+(x)\big) \tag{3.10}$$

defined as the average of function u on face f. The definitions of jump and average are illustrated in figure 3.3a.

A simple calculation rule with jump and average of two functions is handy and easy to proof:

$$[f\, g] = \langle f \rangle [g] + [f] \langle g \rangle \tag{3.11}$$

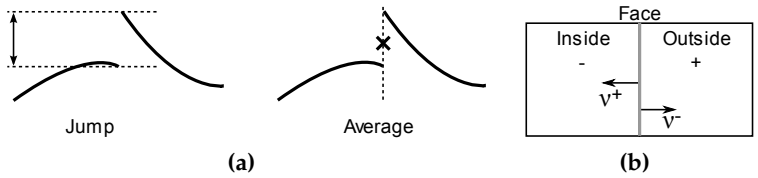

Figure 3.3: (a) Illustration of jump and average of a function and (b) outer normal $\nu^- = \nu$

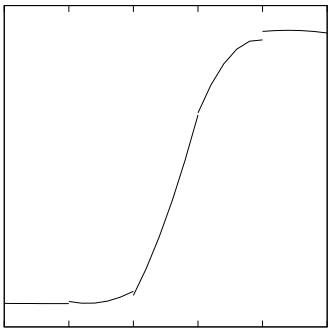

Figure 3.4: Solution with a Discontinuous Galerkin method; jumps on faces and higher-order ansatz functions are visible

3.3 Discontinuous Galerkin methods

Discontinuous Galerkin (DG) methods have an ample theoretical foundation. In the following only an overview is given, which must be understood in the context of other Galerkin methods like standard finite element methods.

DG has basis functions of higher order similar to FEM to get higher convergence rates. Like finite volume methods DG methods conserves the mass locally which is stringently needed for many physical simulations. Finite volume methods and DG methods are discontinuous on element faces, an example for DG methods is given in figure 3.4.

Various different DG methods have been proposed over the last 30 years. [ABC$^+$2002] describes an unified analysis for many methods and provides an extensive list of references for further reading. In this work three closley releated DG methods are used: Symmetrical Interior Penalty Galerkin method (SIPG), Non-symmetrical Interior Penalty Galerkin method (NIPG) and the scheme from Oden, Babuška and Baumann (OBB).

3.3.1 Derivation of the DG methods

A solution must satisfy the equations from the problem formulation in every point. It is reasonable to weaken this requirement and exclude small portions in a defined manner. The derivation of DG methods uses these weak solutions which require test functions and the larger function spaces like $H^1(\Omega)$. This is analog to the approach with FEM, see [Bra2007] for more details.

Based on equation (2.16) a partial integration is made with test functions $v_\alpha \in V_\alpha := \{v \in H^1(\Omega) \big| \, v|_{\partial\Omega_{D,\alpha}} = 0\}$. Because the solution is not continuous on faces the partial integration must be done element by element. Taking into account the boundary conditions this yields

$$\begin{aligned} \frac{\partial}{\partial t} \sum_{e \in E} \int_e \Phi \rho_\alpha S_\alpha v_\alpha \,\mathrm{d}x - \sum_{e \in E} \int_e (\rho_\alpha u_\alpha) \cdot \nabla v_\alpha \,\mathrm{d}x + \sum_{f \in F} \int_f [\rho_\alpha \, u_\alpha \cdot \nu \, v_\alpha] \,\mathrm{d}s \\ = \sum_{e \in E} \int_e q_\alpha v_\alpha \,\mathrm{d}x - \sum_{f \in F_{N,\alpha}} \int_f j_\alpha v_\alpha \,\mathrm{d}s \qquad \text{for all } v_\alpha \in V_\alpha. \end{aligned} \tag{3.12}$$

The jump over the faces can be split up with (3.11)

$$[\rho_\alpha \, u_\alpha \cdot \nu \, v_\alpha] = [\rho_\alpha \, u_\alpha \cdot \nu] \langle v_\alpha \rangle + \langle \rho_\alpha \, u_\alpha \cdot \nu \rangle [v_\alpha]. \tag{3.13}$$

The normal component of $\rho_\alpha u_\alpha$ is continous almost everywhere on the face, hence the jump of $\rho_\alpha \, u_\alpha \cdot \nu$ vanishes almost everywhere on the face

$$\sum_{f \in F} \int_f \underbrace{[\rho_\alpha \, u_\alpha \cdot \nu]}_{=0 \text{ a. e.}} \langle v_\alpha \rangle = 0. \tag{3.14}$$

With the gained simplification from (3.13) and (3.14) equation (3.12) can be written as

$$\begin{aligned} \frac{\partial}{\partial t} \sum_{e \in E} \int_e \Phi \rho_\alpha S_\alpha v_\alpha \,\mathrm{d}x - \sum_{e \in E} \int_e (\rho_\alpha u_\alpha) \cdot \nabla v_\alpha \,\mathrm{d}x + \sum_{f \in F} \int_f \langle \rho_\alpha \, u_\alpha \cdot \nu \rangle [v_\alpha] \,\mathrm{d}s \\ = \sum_{e \in E} \int_e q_\alpha v_\alpha \,\mathrm{d}x - \sum_{f \in F_{N,\alpha}} \int_f j_\alpha v_\alpha \,\mathrm{d}s \qquad \text{for all } v_\alpha \in V_\alpha. \end{aligned} \tag{3.15}$$

Substituting $-\lambda_\alpha K (\nabla p_\alpha - \rho_\alpha g)$ for u_α according to Darcy's law (2.17) gives

$$\begin{aligned} \frac{\partial}{\partial t} \sum_{e \in E} \int_e \Phi \rho_\alpha S_\alpha v_\alpha \,\mathrm{d}x + \sum_{e \in E} \int_e \left(\rho_\alpha \lambda_\alpha K (\nabla p_\alpha - \rho_\alpha g)\right) \cdot \nabla v_\alpha \,\mathrm{d}x \\ + \sum_{f \in F} \int_f \big\langle - \rho_\alpha \lambda_\alpha K (\nabla p_\alpha - \rho_\alpha g) \cdot \nu \big\rangle [v_\alpha] \,\mathrm{d}s \\ = \sum_{e \in E} \int_e q_\alpha v_\alpha \,\mathrm{d}x - \sum_{f \in F_{N,\alpha}} \int_f j_\alpha v_\alpha \,\mathrm{d}s \qquad \text{for all } v_\alpha \in V_\alpha. \end{aligned} \tag{3.16}$$

3.3.2 Stabilization

The resulting method would not be stable. SIPG, NIPG and OBB use a term, which is similar to the diffusive fluxes over faces, to stabilize the method. DG methods differ in this artificial term. Apart from these DG methods not all resulting methods are stable or consistent.

Seperating the diffusive and the convective fluxes:

$$\left\langle -\rho_w \lambda_w K \left(\nabla p_w - \rho_w g\right) \cdot \nu \right\rangle [v_p] = \underbrace{-\left\langle \rho_w \lambda_w K \nabla p_w \cdot \nu \right\rangle [v_p]}_{\text{Diffusive flux}} + \underbrace{\left\langle \rho_w^2 \lambda_w K g \cdot \nu \right\rangle [v_p]}_{\text{Convective flux}} \tag{3.17}$$

The numerical flux

$$\varepsilon \left\langle \rho_w \lambda_w K \nabla v_p \cdot \nu \right\rangle [p_w] \tag{3.18}$$

is added for stabilization in pressure equation. When the sign $\varepsilon \in \{-1, 1\}$ is negative, (3.18) is symmetric to (3.17) like in SIPG. NIPG and OBB use a positive numerical flux.

To reduce the width of jumps in SIPG and NIPG an additional penalty term is introduced:

$$\frac{\sigma}{|f|^\beta} \int\limits_{f \in F} [p_w][v_p] \, \mathrm{d}s \tag{3.19}$$

The penalty term scales with the reciprocal size of space discretization h^{-1} because it is divided by the length of the face $|f|$.

Analogously in the saturation equation, the diffusive flux is identified

$$\begin{aligned} &\left\langle -\rho_n \lambda_n K \left(\nabla p_w + \nabla p_c (1 - S_n) - \rho_n g\right) \cdot \nu \right\rangle [v_S] = \\ &\quad \underbrace{-\left\langle \rho_n \lambda_n K \nabla p_c (1 - S_n) \cdot \nu \right\rangle [v_S]}_{\text{Diffusive flux}} + \underbrace{\left\langle \rho_n \lambda_n K \left(-\nabla p_w + \rho_n g \cdot \nu\right) \right\rangle [v_S]}_{\text{Convective flux}} \end{aligned} \tag{3.20}$$

and the numerical flux

$$\varepsilon \left\langle \rho_n \lambda_n K \nabla v_S \cdot \nu \right\rangle [p_c (1 - S_n)] \tag{3.21}$$

is added. The penalty weight

$$\frac{\sigma}{|f|^\beta} \int\limits_{f \in F} [p_c (1 - S_n)][v_S] \, \mathrm{d}s \tag{3.22}$$

is also used in the saturation equation for SIPG and NIPG.

The jump of the non-wetting pressure $p_w + p_c(1 - S_n)$ can be used instead of $p_c(1 - S_n)$. [Eps2007] choose it that way. It is not clear which approach leads to better numerical results.

	ε	σ	β
SIPG	-1	$\in (2Kk^2, 5Kk^2)$	$4 \cdot 0.5^d$
NIPG	1	$\in (2K, 5K)$	$4 \cdot 0.5^d$
NIPG over-penalized	1	$\in (2K, 5K)$	$4 \cdot 0.5^d + 2k$
OBB	1	0	-

Table 3.1: DG methods and their constants as used in this work with absolute permeability K, polynomial degree of ansatz functions k and dimension d

Table 3.1 contains possible ranges for the constants ε, σ and β which are mainly chosen according to [Eng2009]. The upper limit of the penalty term for SIPG ensures that the resulting bilinear form is coercive. NIPG always has coercive bilinear forms. Higher penalty values are possible but lead to bad conditioned matrices.

With these two supplementary terms SIPG and NIPG are stable. OBB is stable, if the ansatz functions have at least the polynomial degree $k = 2$.

The expected convergence rate for SIPG in the L^2 norm is $\|u - u_h\|_{L^2} \in \mathcal{O}(h^{k+1})$. NIPG and OBB lose one order of convergence if k is even. With over-penalization, i.e. the scaling of the penalty term is changed from h^{-1} to h^{-2k-1}, NIPG can gain full convergence back for even k.

3.3.3 Borders and upwinding

Border faces with Dirichlet boundary conditions are handled similar to faces inside the domain. The jump over the face is replaced with the difference between the solution and the boundary value $p_w - g_{p_w}$ and $p_c(1 - S_n) - p_c\left(g_{S_w}\right)$. The whole term is given below.

Border faces with Neumann boundary conditions are handled like in the FEM method. The same applies to sources q_α.

To improve the result on faces, upwinding can be used. On both sides of a face the same mobility λ_α^* is chosen, depending on direction of the flux average $\omega_\alpha := -\langle K\left(\nabla p_\alpha - \rho_\alpha g\right)\rangle$.

$$\lambda_\alpha^*(S_\alpha) = \begin{cases} \lambda_\alpha^+(S_\alpha) & \text{for } \omega_\alpha \cdot \nu \geq 0 \\ \lambda_\alpha^-(S_\alpha) & \text{else} \end{cases} \tag{3.23}$$

3.3.4 Fully implicit DG scheme

This section gives the complete formula for the pressure/saturation formulation from (2.19) with the DG schemes and implicit Euler method. Known from the last step are p_w^{i-1} and S_n^{i-1},

the independent unknowns are p_w^i and S_n^i. The equations must be valid for all test functions $v_p \in V_p$ and $v_S \in V_S$.

Pressure equation / wetting phase:

$$\begin{aligned}
&\frac{1}{\Delta t} \int_{e\in E} \Phi \left(\rho_w^t \left(1 - S_n^t\right) - \rho_w^{t-1} \left(1 - S_n^{t-1}\right)\right) v_p \,\mathrm{d}x + \int_{e\in E} \rho_w^t \, \lambda_w^t \, K \left(\nabla \, p_w^t - \rho_w^t \, g\right) \cdot \nabla v_p \\
&+ \int_{f\in F} \varepsilon \left\langle \rho_w^t \, \lambda_w^t K \nabla v_p \cdot \nu \right\rangle [p_w^t] - \left\langle \rho_w^t \, \lambda_w^t \, K \, \nabla p_w^t \cdot \nu \right\rangle [v_p] + \frac{\sigma}{|f|^\beta} [p_w^t][v_p] \,\mathrm{d}s \\
&+ \int_{f\in F_{D,w}} \varepsilon \, \rho_w^t \lambda_w^t K \nabla v_p \cdot \nu \left(p_w^t - g_{p_w}^t\right) - \rho_w^t \, \lambda_w^t \, K \, \nabla p_w^t \cdot \nu \, v_p + \frac{\sigma}{|f|^\beta} (p_w^t - g_{p_w}^t) v_p \,\mathrm{d}s \\
&- \int_{e\in E} q_w \, v_p \,\mathrm{d}x + \int_{f\in F_{N,w}} j_n \, v_p \,\mathrm{d}s
\end{aligned} \tag{3.24}$$

Saturation equation / non-wetting phase:

$$\begin{aligned}
&\frac{1}{\Delta t} \int_{e\in E} \Phi \left(\rho_n^t \, S_n^t - \rho_n^{t-1} \, S_n^{t-1}\right) v_S \,\mathrm{d}x + \int_{e\in E} \rho_n^t \, \lambda_n^t \, K \left(\nabla \, p_w^t + \nabla p_c^t - \rho_n^t \, g\right) \cdot \nabla v_S \\
&+ \int_{f\in F} \varepsilon \, \left\langle \rho_n^t \lambda_n^t \, K \, \nabla v_S \cdot \nu \right\rangle [p_c^t] - \left\langle \rho_n^t \lambda_n^t \, K \, \left(\nabla p_w^t + \nabla p_c^t\right) \cdot \nu \right\rangle [v_S] + \frac{\sigma}{|f|^\beta} [p_c^t][v_S] \,\mathrm{d}s \\
&+ \int_{f\in F_{D,n}} \varepsilon \, \rho_n^t \lambda_n^t \, K \, \nabla v_S \cdot \nu \, \left(p_c(S_n^t) - p_c\left(g_{S_n}^t\right)\right) - \rho_n^t \, \lambda_n^t \, K \, \left(\nabla p_w^t + \nabla p_c^t\right) \cdot \nu \, v_S \\
&\qquad + \frac{\sigma}{|f|^\beta} \left(p_c(S_n^t) - p_c\left(g_{S_n}^t\right)\right) v_S \,\mathrm{d}s \\
&- \int_{e\in E} q_n \, v_S \,\mathrm{d}x + \int_{f\in F_{N,n}} j_n \, v_S \,\mathrm{d}s
\end{aligned} \tag{3.25}$$

The gradient of capillary pressure $\nabla p_c(S)$ is often unknown and must be calculated numerically. In this work $p_c'(S) \, \nabla S$ is used because p_c is given analytically.

This scheme is fully implicit, it must be solved as one large non-linear system.

The pressure/pressure formulation from (2.24) can be obtained by using the wetting phase equation (3.24) twice, for the wetting phase and for the non-wetting phase with index n instead of w.

3.4 Further improvements

3.4.1 Weighted averages

Different types of soil can meet closely and cause large jumps in permeability. The jumps of several orders of magnitude are difficult to handle numerically. Discontinuous solutions are likely. When the space is discretized, the border between the types of soil should be a face and not inside an element. Then solutions from DG methods can have discontinuities on faces, too. From now on only different permeabilities along faces are considered.

To allow wider jumps [ESZ2009] proposes weighted averages. They are a harmonic mean of the different permeabilities and a smaller penalty factor for the face.

Let K^- and K^+ be defined as the absolute permeabilities on the inside and outside of a face $f \in F$. With $\delta_{K\nu}^{\pm} := \nu^{\mathsf{T}} K^{\pm} \nu$ the factors

$$\omega^+ := \frac{\delta_{K\nu}^-}{\delta_{K\nu}^+ + \delta_{K\nu}^-} \qquad \text{and} \qquad \omega^- := \frac{\delta_{K\nu}^+}{\delta_{K\nu}^+ + \delta_{K\nu}^-} \tag{3.26}$$

are defined. On the inside and outside of f

$$u_\omega := \omega^+ \lambda^+ K^+ \nabla p^+ + \omega^- \lambda^- K^- \nabla p^- \tag{3.27}$$

is used as the new Darcy's velocity. The factor to lower the penalty term is

$$\gamma_K := \frac{\delta_{K\nu}^+ \delta_{K\nu}^-}{\delta_{K\nu}^+ + \delta_{K\nu}^-}. \tag{3.28}$$

Note that $2\gamma_K$ is the harmonic mean of the velocity in the direction of ν.

As indicated in the conclusions, the averaging from [EMS2010] would be the better choice for two-phase flows in porous media because discontinuous capillary pressures are also included.

3.4.2 Slope limiters

If a solution contains steep fronts, overshots and oscillations can occur near these fronts. These effects differ from the seeked solution, may make further steps more difficult to calculate and are unphysical in applications. Slope limiters are often used to reduce them. Slope limiters try to detect changes between steep and even parts, so as to limit the gradient. No slope limiter works for all cases and the right one must be found.

Figure 3.5b shows a solution with a steep front at different points of time, with and without a slope limiter. The solution with slope limiter only has small overshots left. But with increasing time from right to left the positions of the fronts differ more and more. In this work slope limiters are not used.

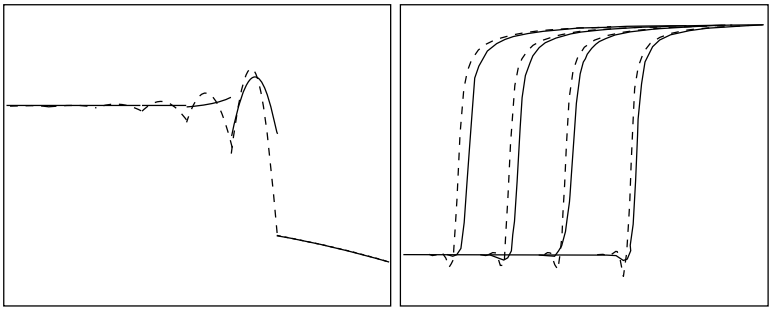

(a) (b)

Figure 3.5: (a) Solid line with weighted averages, dotted line without (b) Solutions at different points of time for an infiltration front entering from right to left; solid line with slope limiter, dotted line without, after [Soc2008]

3.4.3 Velocity reconstruction

The normal component of Darcy's velocity $\rho_\alpha u$ is almost everywhere continuous. The DG methods in this work do not honor this fact. With an additional velocity reconstruction this deficit can be removed. An interpolation to other elements which are coupled by the normal component over the faces, like Ravier-Thomas elements, is made after every time step. This reduces oscillations which occur if the two equations are not solved fully implicitly but sequentially equation by equation. [EMS2009] shows the gained improvement of a velocity reconstruction.

4 Software

Many algorithms or tools are necessary to solve partial differential equations: Linear and non-linear solvers which solve huge systems in reasonable time, a grid manager to handle the mesh, functions for the ansatz and test spaces, quadrature rules, ways to visualize results, possibilities for parallel computation and many more. The development of an up to date solver software from scratch takes several man-years. The next sections present the softwares DUNE and PDELab which are used. The last section describes the program which was written in the course of the present work.

4.1 DUNE

DUNE is a C++ library to solve partial differential equations with mesh based methods, see [BBD+2008b], [BBD+2008a] and figure 4.1a. The development started in 2002 due to the lack of flexible and maintainable but still fast software. DUNE is under an open source licence and is actively developed by a couple of universities.

The main goals of flexibility and speed are achieved by the use of C++ and its template techniques. Today it is common to use abstraction with object oriented programming. Most programming languages provide mechanisms to write and use objects. This is a key to keep one's code maintainable and flexible. But object oriented programs are slower because the abstract code is resolved in run-time. In most cases this is justifiable. In numerical software the code inside a loop or function can run through several thousands times and the object handling dominates the execution time of the actual calculation. Template meta-programming and static polymorphism can emulate most advantages of object oriented programming. As templates are evaluated by the compiler, the programs become faster at the cost of longer compiler runs.

DUNE comprises of several modules. Classes for vectors, matrices and parallel computing are provided by dune-common. Iterative solvers, preconditioners and facades to other solver libraries are in dune-istl. Simple grids and wrappers to external grids are contained in dune-grid. With dune-localfunctions a rich pool of functions is available.

Research groups often get stuck with older programs that have been growing over time. It is possible to integrate these legacy programs to make the migration to DUNE easier or to develop them independently. For example most grid managers are separately developed and older than DUNE.

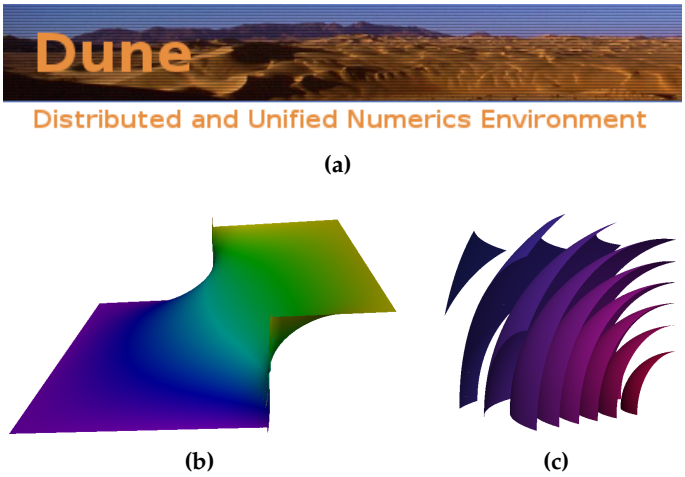

Figure 4.1: (a) Logo of the DUNE project, [NNc] (b) Solution of two-dimensional elliptic problem (c) Isosurfaces in a three-dimensional solution

4.2 PDELab

The versatility of DUNE causes some complexity and makes it difficult to learn its use. PDELab is an additional abstraction layer which was created to spread DUNE more in academic and application use. The module stays close to mathematical formulation of numerical methods. It keeps a local view to an element or a face and the user does not need to handle grid details. Only a function space and a grid manager must be chosen, then PDELab assembles and solves stiffness matrix and load vector automatically.

As a DUNE module it uses the other modules and the programs are compatible to other DUNE software. PDELab is being developed since February 2009 and is not yet released. [BHM2010] covers PDELab in more detail.

4.3 Solvers for two-phase flows in porous media

The high level of provided functionality from PDELab made it possible to cope with the work within the relativly short span of six months. In the context of this work several solvers for the two-phase problem were written. The Richards equation can be solved with FEM and the three DG methods described earlier. To solve the pressure/pressure or the pressure/saturation formulation FEM solvers were programmed. For the pressure/saturation formulation a DG code was written, too, but the SIPG method does not work.

The programs to solve the Richards equation use Crank-Nicolson for time discretization or, the two-phase flows solvers implicit Euler. The space is discretized with a structured

rectangular grid and the methods given above. Other grids can be used but this sufficed in all examples. All FEM codes use Q1 or Q2 basis functions, the DG codes monomes. The programs do not contain velocity reconstruction. The two-phase flows solver uses upwinding for the mobilites λ_α. Weighted averages are implemented as in [ESZ2009]. Slope limiters are not implemented, only the effective saturation $\bar{S}_\alpha$ are limited in the range of 0 and 1 when evaluating the relative permeability $k_{r\alpha}$ and the capillary pressure p_c, because otherwise they are not defined.

The occurring linear systems of equations are solved with the LU decomposition of SuperLU. The systems of equations are small enough to solve them quickly and it avoids additional problems from an iterative solver for asymmetric matrices. The built-in Newton solver is used for non-linear systems of equations. It uses an enhancement called line search or damped Newton to reduce the needed Newton iteration steps and to make it more stable, as described in [Bra2007].

All programs can be used in one, two or three dimensions. The used grid manager does not support higher dimension, thus this remains untested.

It is intended to commit at least simplified versions of these programs to the PDELab examples.

5 The Richards equation

In this chapter numerical results for the Richards equation are calculated to back the aimed correctness of the program. The test cases are taken from papers and are borrowed from [Soc2008].

5.1 The Haverkamp example

Haverkamp et al. compared in [HVT+1977] different discretizations for the nonlinear infiltration equation. Many researches have used one of their examples like [CBZ1990, MF2004] and [Soc2008]. The Haverkamp example qualifies as a first test because it does not raise any numerical difficulties and has been independently reproduced with different numerical methods, which were verified by experimentally measured data.

The test case models vertical water infiltration in the unsaturated region of ground. The whole domain is filled with a constant hydraulic head and the ground is made of sand. Through the top water infiltrates the domain, leading to a higher pressure floating downwards. The example lasts for ten minutes. It is an one-dimensional example with a height of 40 cm as sketched in Figure 5.1a.

The following formulae describe the saturation

$$S(p) = \frac{\theta_s - \theta_r}{1 + |0.027\,1/\mathrm{cm}\; p|^{3.96}} + \theta_r \tag{5.1}$$

with $\theta_s = 0.287$ and $\theta_r = 0.075$ as well as the conductivity

$$K(p) = I\,\frac{K_s}{1 + |0.0524\,1/\mathrm{cm}\; p|^{4.74}} \tag{5.2}$$

with $K_s = 9.44 \cdot 10^{-3}\,\mathrm{cm/s}$ and are shown in Figures 5.1b and 5.1c. These two functions keep the example simple because they do not contain steep gradients. The domain Ω, the source term q, the initial and the boundary conditions are given by

$$\begin{aligned}
\Omega &= [0\,\mathrm{cm}, 40\,\mathrm{cm}] \\
T &= 10\,\mathrm{min} = 600\,\mathrm{s} \\
q &= 0 \\
p(\cdot, 0\,\mathrm{s}) &= -61.5\,\mathrm{cm} \\
p(40\,\mathrm{cm}, \cdot) &= -20.7\,\mathrm{cm} \\
p(0\,\mathrm{cm}, \cdot) &= -61.5\,\mathrm{cm}.
\end{aligned}$$

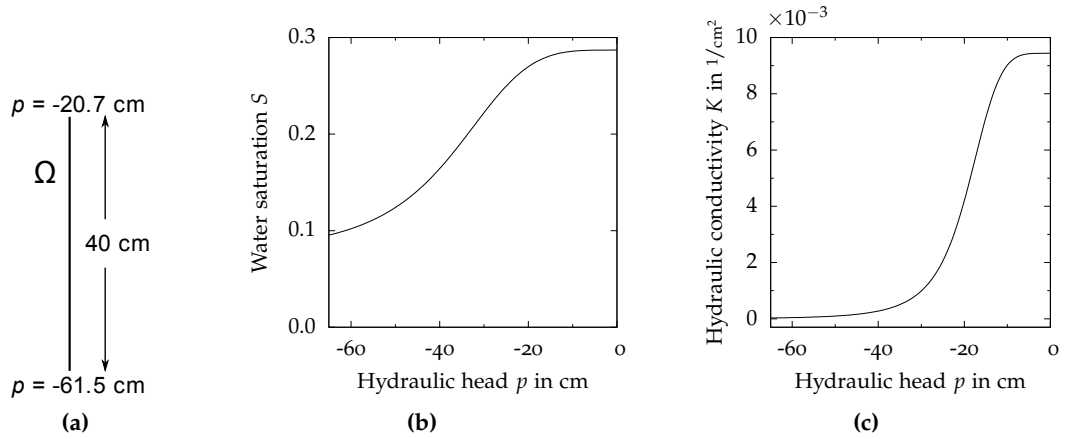

Figure 5.1: (a) Layout, (b) saturation and (c) conductivity for the Haverkamp example

As shown in Figure 5.2 the water enters at the top and infiltrates towards the bottom. In the figures the domain is rotated to flow right to left. All simulations are reasonably close to the expected result in regard to the coarse grid with only 16 elements. Some higher ordered methods need smaller time steps to converge. In some plots an unphysical overshot below $-61.5\,\mathrm{cm}$ is visible because the solution is steep and no slope limiter is used. NIPG and OBB show jumps between elements while FEM is continuous and SIPG has invisibly small jumps.

The results look similar compared to the articles cited above.

5.2 Example with analytic solution

The quality of the results with the Haverkamp example cannot be measured. Quality estimates are established based only on unphysical behavior and visible variations between solutions made with different numerical methods or experimentally measured data. If the solution is known, an error can be calculated. As shown in [EG2004] an error norm and its convergence rate for linear parabolic partial differential equations with a smooth enough solution and k the order of the basis functions is

$$\|p_h(\cdot,T) - p(\cdot,T)\|_{L^2(\Omega)} \in \mathcal{O}\left(h^k + \Delta t\right). \tag{5.3}$$

In the following chapter this will be called L^2 *norm*.

A second norm and its expected convergence rate is

$$\int_0^T \|\nabla p_h(\cdot,t) - \nabla p(\cdot,t)\|_{L^2(\Omega)}\,\mathrm{d}t \in \mathcal{O}\left(h^{k-1} + \Delta t\right) \tag{5.4}$$

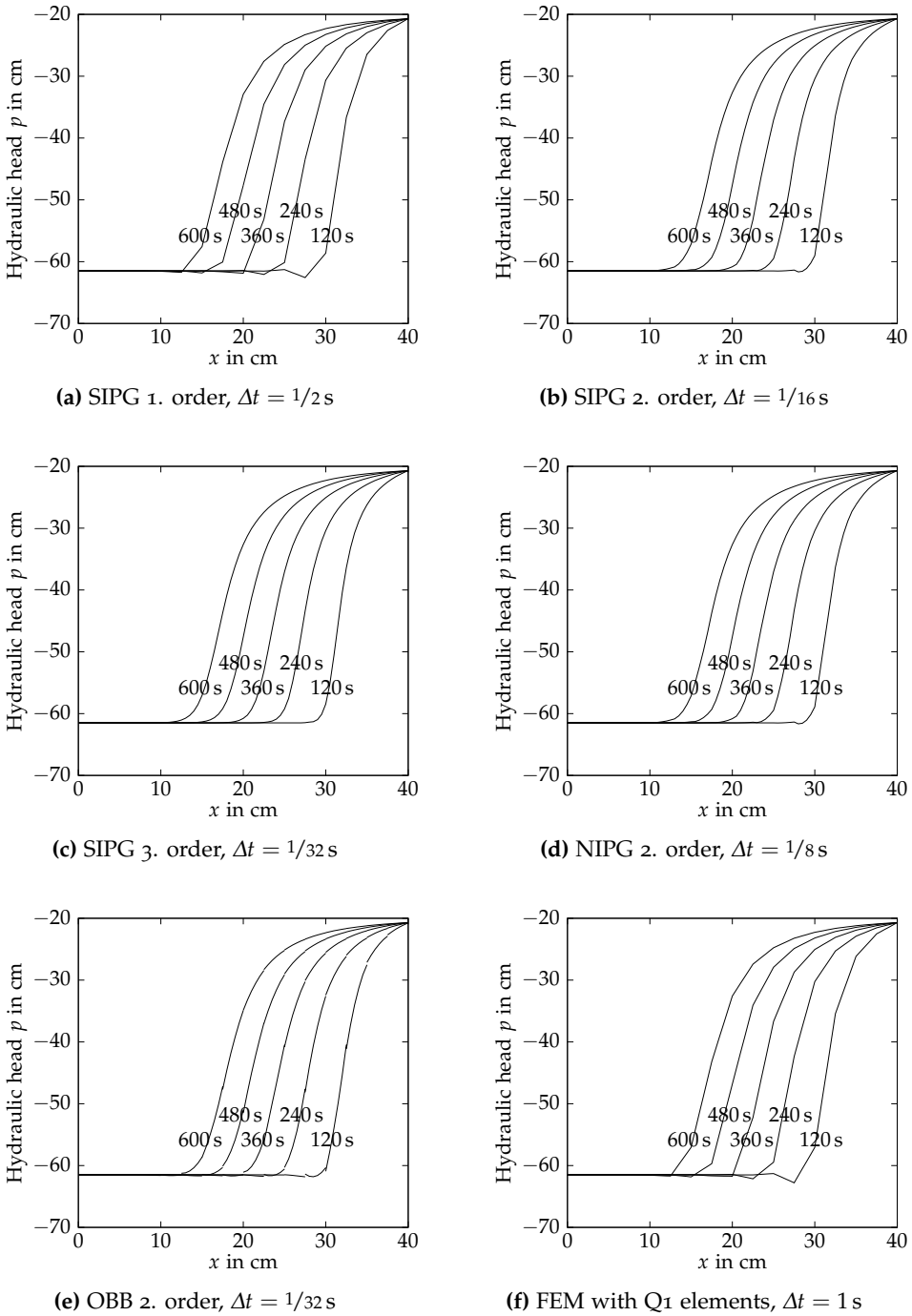

(a) SIPG 1. order, $\Delta t = 1/2\,\mathrm{s}$

(b) SIPG 2. order, $\Delta t = 1/16\,\mathrm{s}$

(c) SIPG 3. order, $\Delta t = 1/32\,\mathrm{s}$

(d) NIPG 2. order, $\Delta t = 1/8\,\mathrm{s}$

(e) OBB 2. order, $\Delta t = 1/32\,\mathrm{s}$

(f) FEM with Q1 elements, $\Delta t = 1\,\mathrm{s}$

Figure 5.2: Solutions of the Haverkamp example with different methods, every 120 s. From (a) to (c) the basis functions' order increases with SIPG. For comparison (d), (e) and (f) show other methods. All simulations were done with $h = 40/16\,\mathrm{cm}$.

which will be named *integrated L^2 norm*.

One can assume similar results with these Richards equation examples.

This example is taken from [Soc2008] and is a modification of Haverkamp example. It provides an analytic solution

$$p_a(x,t) = 20.4 \tanh\left(0.5 \left(x + \frac{t}{12} - 15\right)\right) - 41.1. \tag{5.5}$$

To make the computation faster the domain Ω is smaller and duration T is shorter.

$$\begin{aligned} \Omega &= [0\,\mathrm{cm}, 20\,\mathrm{cm}] \\ T &= 100\,\mathrm{s} \\ p(\cdot, 0\,\mathrm{s}) &= p_a(\cdot, 0\,\mathrm{s}) \\ p(20\,\mathrm{cm}, \cdot) &= -20.7\,\mathrm{cm} \\ p(0\,\mathrm{cm}, \cdot) &= -61.5\,\mathrm{cm}. \end{aligned}$$

The functions describing saturation and conductivity remain the same as in the Haverkamp example, see (5.1) and (5.2). The source term q forces the last example's solution to become p_a. It is elongate and can be found in Appendix A.

Numerical results are shown in Figure 5.3. The mesh refinements in Figures 5.3a and 5.3b with SIPG matches the expectations from above as well as the expected convergence rates for ansatz functions with increasing order. The integrated L^2 error decreases notably slower. NIPG without over-penalization and OBB lose one order in the convergence rate with an even ansatz functions' order k. This is visible in Figure 5.3c.

The time discretization is examined in Figures 5.3e and 5.3f. Crank-Nicolson provides a convergence rate of 2 which is reached with both norms; the independence of the space discretization is shown. Unlike all other examples the graphs were not cut off when the error of space discretization dominated, because usually it perturbs the graphs and distracts from the result. Figure 5.3d demonstrates the lower convergence rate of the implicit Euler scheme compared to the Crank-Nicolson scheme, according to theoretical knowledge.

5.3 Example with variable saturation and analytic solution

This example is roughly the same as the last one but the saturation increases faster to pass the crossing between the unsaturated and saturated regions.

To increase the saturation faster a term $\frac{t}{4}$ is added to the analytic solution:

$$p_{\tilde{a}}(x,t) = 20.4 \tanh\left(0.5 \left(x + \frac{t}{12} - 15\right)\right) + \frac{t}{4} - 41.1. \tag{5.6}$$

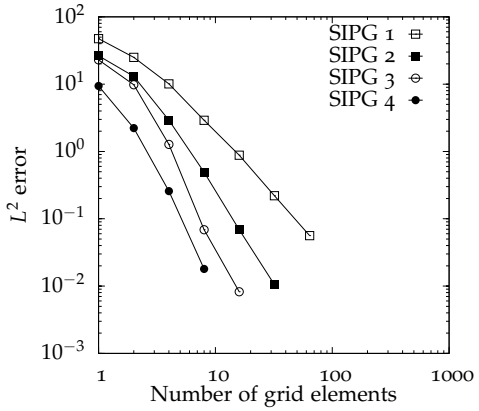

(a) $\Delta t = 1/6400$ s

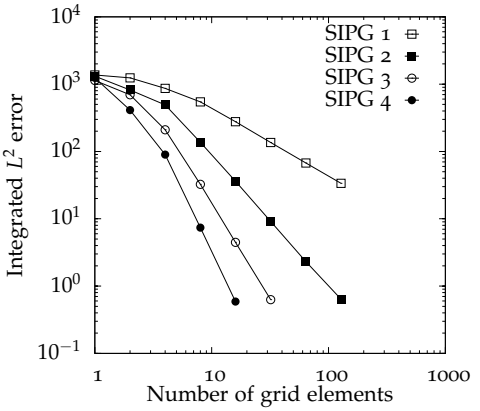

(b) $\Delta t = 1/6400$ s

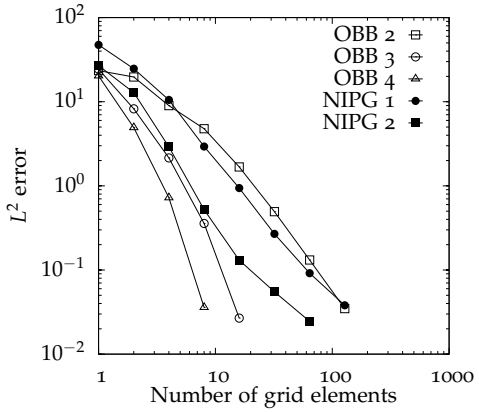

(c) $\Delta t = 1/6400$ s

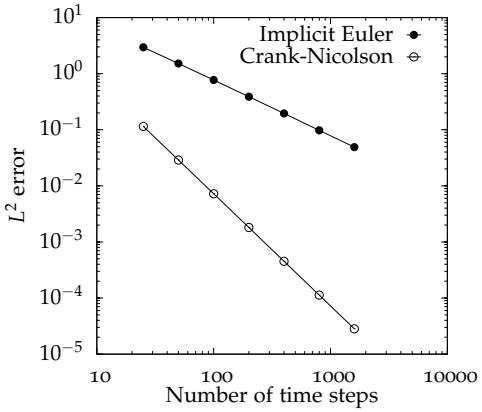

(d) SIPG 3. order, $h = 40/128$ cm

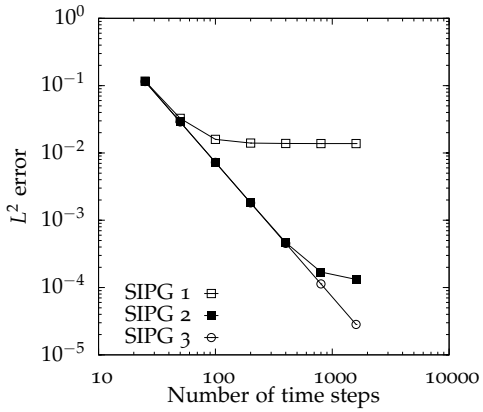

(e) $h = 40/128$ cm

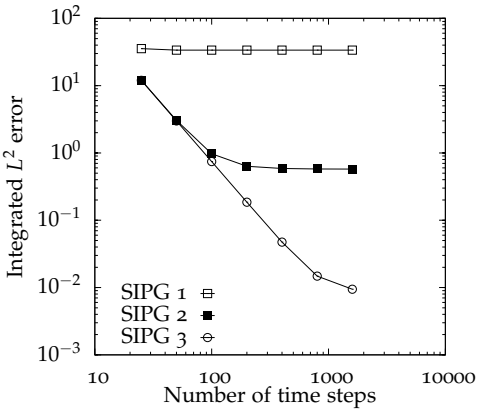

(f) $h = 40/128$ cm

Figure 5.3: (a), (b), (c) mesh refinement and (e), (f), (d) time refinement with different discretizations

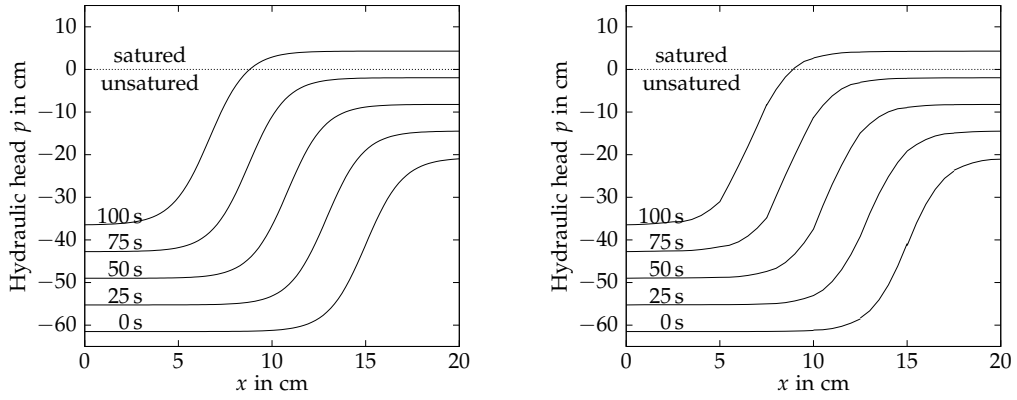

Figure 5.4: (a) Excepted solution at different points of time (b) numerical solution with $\Delta t = 1\,\mathrm{s}$, $h = {}^{20}/_{4}\,\mathrm{cm}$ and 2. order NIPG

Figure 5.4a shows the analytic solution for different points in time.

The changed analytic solution affects the source term $\tilde{q}$ and is given in Appendix A, too.

If the soil is saturated, the saturation S becomes 1 and conductivity K simplifies to K_S. Referring to the functions suggested by Haverkamp et al. in (5.1) and (5.2) the new saturation

$$\tilde{S}(p) = \begin{cases} 1 & \text{if} \quad p \geq 0 \\ S(p) & \text{if} \quad p < 0 \end{cases} \tag{5.7}$$

and the new conductivity

$$\tilde{K}(p) = \begin{cases} K_S & \text{if} \quad p \geq 0 \\ K(p) & \text{if} \quad p < 0 \end{cases} \tag{5.8}$$

are defined. The remaining definitions are

$$\begin{aligned} \Omega &= [0\,\mathrm{cm}, 20\,\mathrm{cm}] \\ T &= 100\,\mathrm{s} \\ p(\cdot, 0\,\mathrm{s}) &= p_{\tilde{a}}(\cdot, 0\,\mathrm{s}) \\ p(20\,\mathrm{cm}, \cdot) &= p_{\tilde{a}}(20\,\mathrm{cm}, \cdot) \\ p(0\,\mathrm{cm}, \cdot) &= p_{\tilde{a}}(0\,\mathrm{cm}, \cdot). \end{aligned}$$

Figure 5.4b shows one result at different time points which can hardly be distinguished from the analytical solution next to it even though the space is only discretized by four

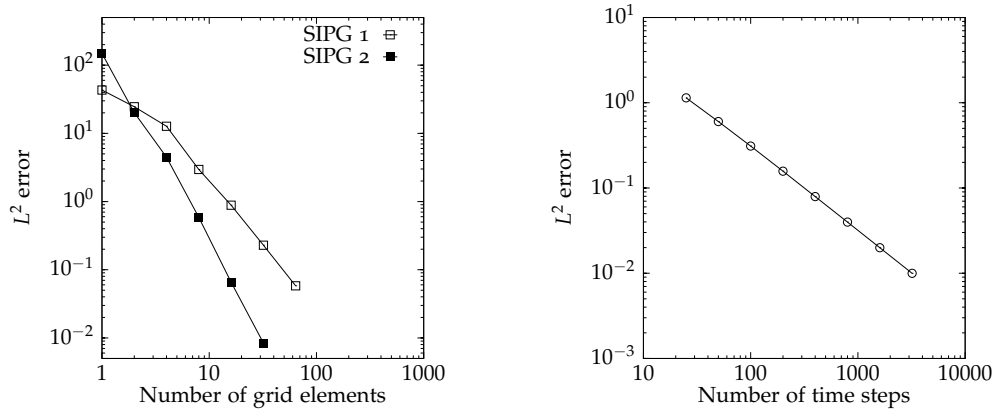

(a) $\Delta t = 1/6400$ s **(b)** SIPG 3. order, Crank-Nicolson, $h = 1/512$ s

Figure 5.5: Error plots for saturated test case with refinement of (a) space and (b) time discretization

elements. The error norms given in Figure 5.5 deliver the theoretical results and look similar to Figure 5.3.

5.4 The Polmann example

The following example is from D. Polmann (1988). It describes approximately a field site in New Mexico with infiltration in unsaturated ground and was published in [CBZ1990]. It served as a test case in [MF2004] and [Soc2008], too.

The Polmann example is similar to Haverkamp's one. It is one-dimensional and water infiltrates from top to bottom. But the pressure wetting front becomes steep which results in a challenging example.

The functions for saturation S and conductivity K are

$$S(p) = \frac{\theta_s - \theta_r}{\left(1 + (\epsilon\,|p|)^n\right)^m} + \theta_r \tag{5.9}$$

and

$$K(p) = K_s \frac{\left(1 - (\epsilon\,|p|)^{n-1}\,\left(1 + (\epsilon\,|p|)^n\right)^{-m}\right)^2}{\left(1 + (\epsilon\,|p|)^n\right)^{\frac{m}{2}}} \tag{5.10}$$

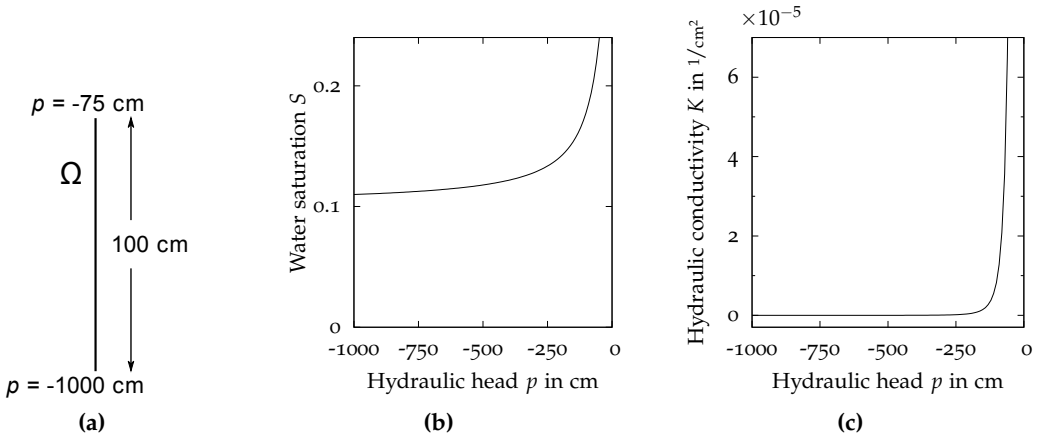

Figure 5.6: (a) Layout, (b) saturation and (c) conductivity for the Polmann example

with $n = 2$, $m = 0.5$, $\epsilon = 0.0335\,{}^{1}/_{\mathrm{cm}}$, $\theta_s = 0.368$, $\theta_r = 0.102$ and $K_s = 9.22 \cdot 10^{-3}\,\mathrm{cm/s}$. Figures 5.6b and 5.6c show both functions. The remaining definitions are

$$\begin{aligned} \Omega &= [0\,\mathrm{cm}, 100\,\mathrm{cm}] \\ T &= 48\,\mathrm{h} = 48 \cdot 60 \cdot 60\,\mathrm{s} \\ p(\cdot, 0\,\mathrm{s}) &= -1000\,\mathrm{cm} \\ p(100\,\mathrm{cm}, \cdot) &= -75\,\mathrm{cm} \\ p(0\,\mathrm{cm}, \cdot) &= -1000\,\mathrm{cm}. \end{aligned}$$

Figure 5.7 shows some numerical results. They look like results from [CBZ1990, MF2004, Soc2008]. SIPG and NIPG show nice results with a few grid elements and keep the steep front, see Figures (a) and (b). With OBB which does not penalize jumps between elements no solution can be found. The Newton solver does not converge when the front leaves the first element.

The non-physical overshot below -1000 cm is present in all results. E.g. with SIPG 2. order and $h = {}^{100}/_{16}\,\mathrm{cm}$ it can reach -1600 cm. If the grid is more refined, the overshot becomes so large that the correct solution is not found anymore.

The steep front and the overshot result from the steep permeability function K. Weighted averages do not work with this example. The solution dependent relative permeability does break this method.

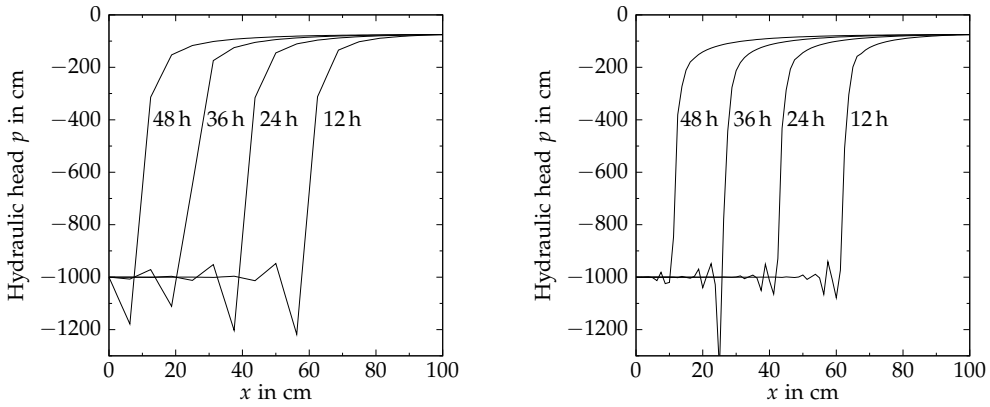

(a) SIPG 1. order, $\Delta t = 60\,\mathrm{s}$, $h = {}^{100}/_{16}\,\mathrm{cm}$

(b) SIPG 3. order, $\Delta t = {}^{60}/_{4}\,\mathrm{s}$, $h = {}^{100}/_{16}\,\mathrm{cm}$

Figure 5.7: Numerical results of the Polmann example at different points of time

6 Two-phase flows in porous media

Numerical results for the two-phase flows are presented in this chapter to validate the numerical model. The saturation/pressure formulation with DG methods is uncommon. To this end examples from sources with other formulations are adapted.

6.1 The Buckley-Leverett example

This one-dimensional Buckley-Leverett example is taken from [ESZ2009], where it is solved with a global pressure formulation. The domain is initially filled with three quarters of non-wetting phase and one quarter of wetting phase. From the left side wetting fluid is pressed into the soil replacing the non-wetting phase.

The Brooks-Corey model is used for capillary pressure

$$p_c(\bar{S}_n) = p_e \left(1 - \bar{S}_n\right)^{-\frac{1}{\lambda}} \tag{6.1}$$

and relative permeabilities

$$k_{rw}(\bar{S}_n) = \left(1 - \bar{S}_n\right)^{\frac{2+3\lambda}{\lambda}} \qquad \text{and} \qquad k_{rn}(\bar{S}_n) = \bar{S}_n^2 \left(1 - \left(1 - \bar{S}_n\right)^{\frac{2+\lambda}{\lambda}}\right) \tag{6.2}$$

with $\lambda = 2$, $p_e = 10^3\,\mathrm{Pa}$, $S_{wr} = 0.2$ and $S_{nr} = 0.15$. Let the porosity be $\phi = 0.2$, the absolute permeability $K = 10^{-11}\,\mathrm{m}^2$, viscosities $\mu_w = 0.001\,\mathrm{kg/m{\cdot}s}$ and $\mu_n = 0.01\,\mathrm{kg/m{\cdot}s}$. No sources or sinks are in the domain, hence $q_w = q_n = 0$. The domain is $\Omega = [0\,\mathrm{m}, 300\,\mathrm{m}]$ as shown in figure 6.1. The simulation lasts for $T = 360\,\mathrm{days} = 60 \cdot 60 \cdot 24 \cdot 360\,\mathrm{s}$. The boundary and initial conditions are

$$\begin{aligned} S_n(0\,\mathrm{m}, \cdot) &= 0.25 & p_w(0\,\mathrm{m}, \cdot) &= 300\,000\,\mathrm{Pa} \\ S_n(300\,\mathrm{m}, \cdot) &= 0.7 & p_w(300\,\mathrm{m}, \cdot) &= 150\,000\,\mathrm{Pa} \\ S_n(\cdot, 0\,\mathrm{s}) &= 0.7. \end{aligned}$$

The results in figure 6.2 match to the pictures in [ESZ2009], only the front is at most 10 % farer right for $t = 360\,\mathrm{days}$. OBB and NIPG coincide with FEM.

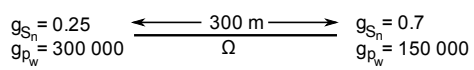

Figure 6.1: Setting of the Buckley-Leverett example

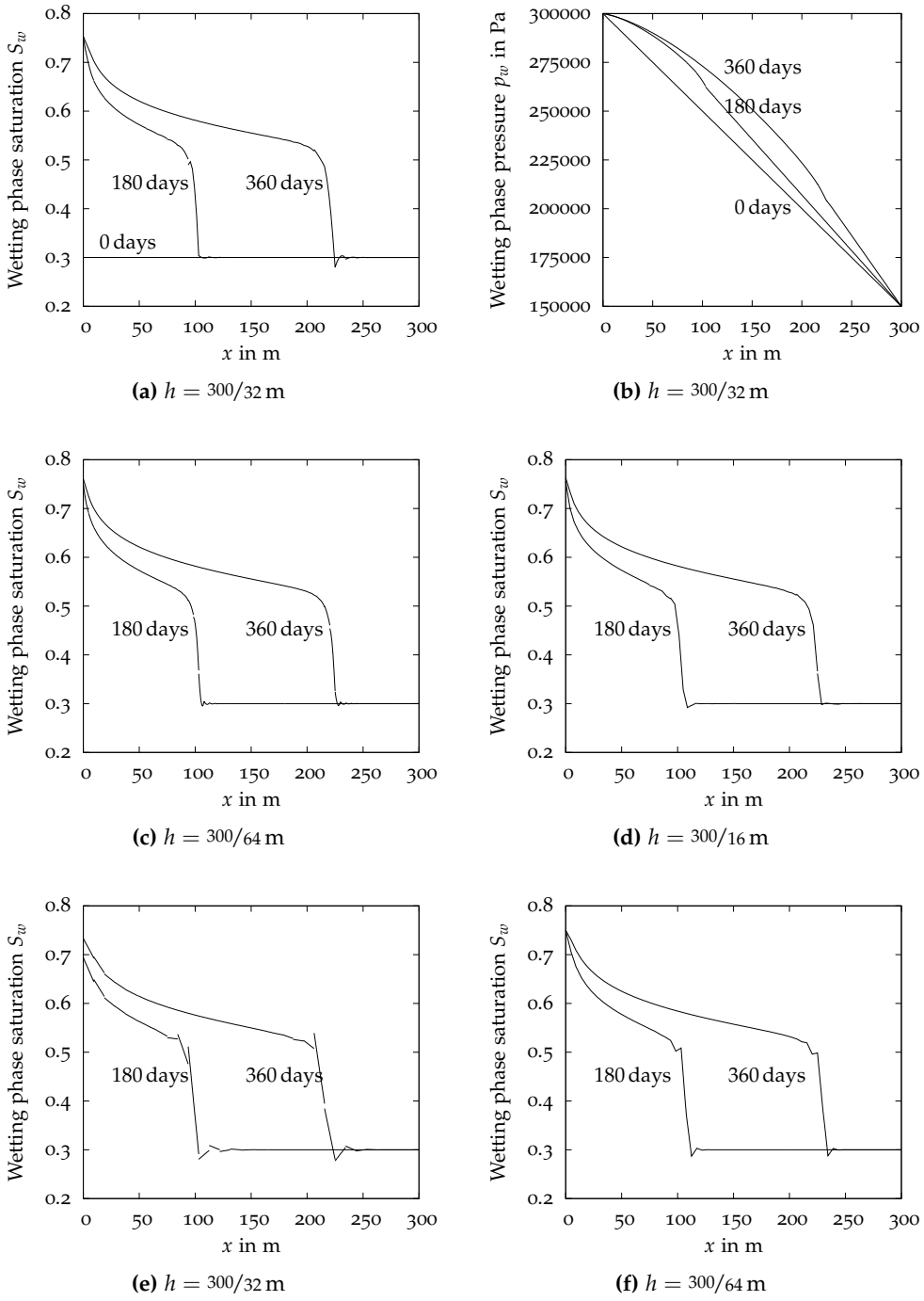

(a) $h = 300/32\,\mathrm{m}$ **(b)** $h = 300/32\,\mathrm{m}$

(c) $h = 300/64\,\mathrm{m}$ **(d)** $h = 300/16\,\mathrm{m}$

(e) $h = 300/32\,\mathrm{m}$ **(f)** $h = 300/64\,\mathrm{m}$

Figure 6.2: The Buckley-Leverett example at different points of time for (a) saturation and (b) pressure with NIPG 2. order (c) OBB 2. order and (c) OBB 5. order (e) NIPG 1. order (f) FEM with Q1 elements, $\Delta t = 3.6\,\mathrm{days}$, $h = 300/32\,\mathrm{m}$

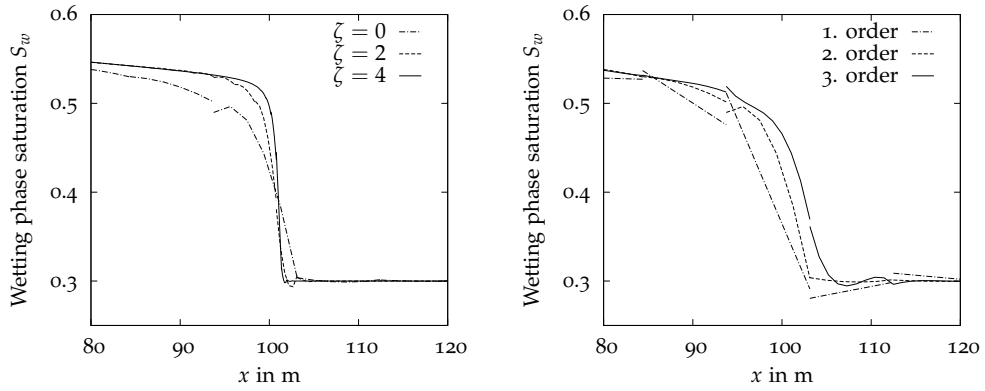

(a) **(b)** $\Delta t = 3.6$ days, $h = {}^{300}/_{62}$ m

Figure 6.3: Detail of the Buckley-Leverett example at $t = 180$ days (a) with refinements in space and time, NIPG 2. order, $\Delta t = {}^{3.6}/_{2^\zeta}$ days, $h = {}^{300}/_{32 \cdot 2^\zeta}$ m and (b) with NIPG of different order

With finer grids and smaller time steps, like in figure 6.3a, the front becomes steeper and oscillations remain locally.

Higher-order methods do not yield better results. The problem must be smooth enough. Figure 6.3b illustrates the absence of a better solution with higher-order methods. In this case it would be more efficient to use lower-order methods and refine the grid instead.

SIPG does not work with any configuration. The Newton iteration does not converge when the front reaches a face. It was neither possible to identify a flaw in the sofware nor to figure a therotical argument out. [Eps2007] states that "our numerical tests show that the SIPG method is very sensitive to the choice of the penalty parameter, which is not the case for the NIPG [..] method." At least one of her examples does not work with SIPG at all. Further analysis would be necessary to decide this problem.

6.2 Sand lense example

The sand lense example is inspired by [Bas1999]. It is a two-dimensional example where the non-wetting phase infiltrates from above. The domain is completely filled with the wetting phase. From the top the non-wetting phase flows in and sinks downwards because of its higher density.

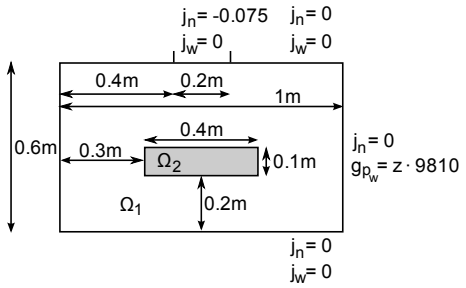

Figure 6.4: Setting of the sand lense problem

6.2.1 Without sand lense

First no lense is inside domain Ω_1. The relative permeabilities are given by

$$k_{rw}(S_w) = \bar{S}_w^2 \qquad \text{and} \qquad k_{rn}(S_n) = (1 - \bar{S}_n)^2 \tag{6.3}$$

with $S_{wr} = S_{nr} = 10^{-6}$. The capillary pressure is

$$p_{c1}(S_w) = p_{e1}\, S_w^{-\frac{2}{5}} \tag{6.4}$$

with $p_{e1} = 755\,\text{Pa}$. The absolute permeability is $K_1 = 6.64 \cdot 10^{-11}\,\text{m}^2$, the porosity $\phi = 0.4$, the viscosities are $\mu_w = 10^{-3}$ and $\mu_n = 0.9 \cdot 10^{-3}$. The boundary and initial conditions are

$$p_w((0\,\text{m}, \cdot), \cdot) = p_w((1\,\text{m}, \cdot), \cdot) = z \cdot 9810\,\text{Pa}$$

$$j_w((x, 0\,\text{m}), \cdot) = \begin{cases} -0.075 & \text{for } x \in [0.4, 0.6] \\ 0 & \text{else} \end{cases}$$

$$j_n(\cdot, \cdot) = 0.$$

The admeasurement is given in figure 6.4. The regular grid has 10×12 elements and is in same cases refined to $10 \cdot 2^l \times 12 \cdot 2^l$ elements. The simulation last $T = 2100\,\text{s}$. If not noted otherwise the timestep is $\Delta t = 35\,\text{s}$.

The results in figure 6.5 match the expectations. The non-wetting phase sinks from the top to the bottom by the gravity force. Diffusive effects broaden the area which contains non-wetting phase. Oscillations are only observable within one element. The solution from FEM is less sharp because more elements around are affected.

6.2.2 With discontinuous permeability

In this example the soil section Ω_1 includes a sand lense. This inclusion Ω_2 is filled with a different material. The capillary pressure inside the lense remains the same. But the absolute

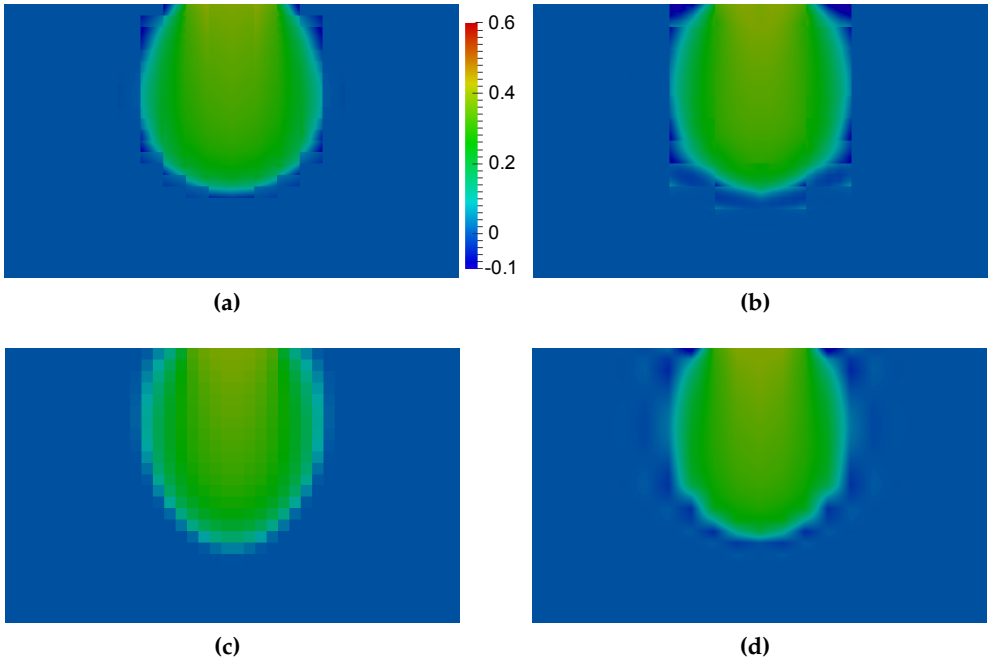

Figure 6.5: Sand lense example without lense at $t = 40 \cdot 35\,\mathrm{s}$ (a) NIPG 1. order with refined grid $l = 1$ (b) OBB 2. order (c) Finite volume on a 40×24 grid (d) FEM with refined grid $l = 1$

permeability in the sand lense is reduced to $K_3 = 3.32 \cdot 10^{-14}\,\mathrm{m}^2$. As a result a choking above the lense occurs.

The numerical results match the expectations. The discontinuous permeability leads to large oszillations which break the solution. The elements below the choking in figures 6.6a and 6.6b are strongly curved; the dark blue strip goes below the lower limit of the color map of 0.1.

Useing the weighted averages the jumps are less penalized and oszillations are reduced. In figure 6.6c the saturation in the sand lense remains unchanged.

6.2.3 With fine sand lense

In this example Ω_2 is filled with fine sand. The sand lense has a different capillary pressure

$$p_{c2}(S_w) = p_{e2}\, S_w^{-\frac{1}{2}} \tag{6.5}$$

and an absolute permeability $K_2 = 3.32 \cdot 10^{-11}\,\mathrm{m}^2$. The infiltrating non-wetting fluid does not enter the sand lense before the pressure difference between outside and inside the lense

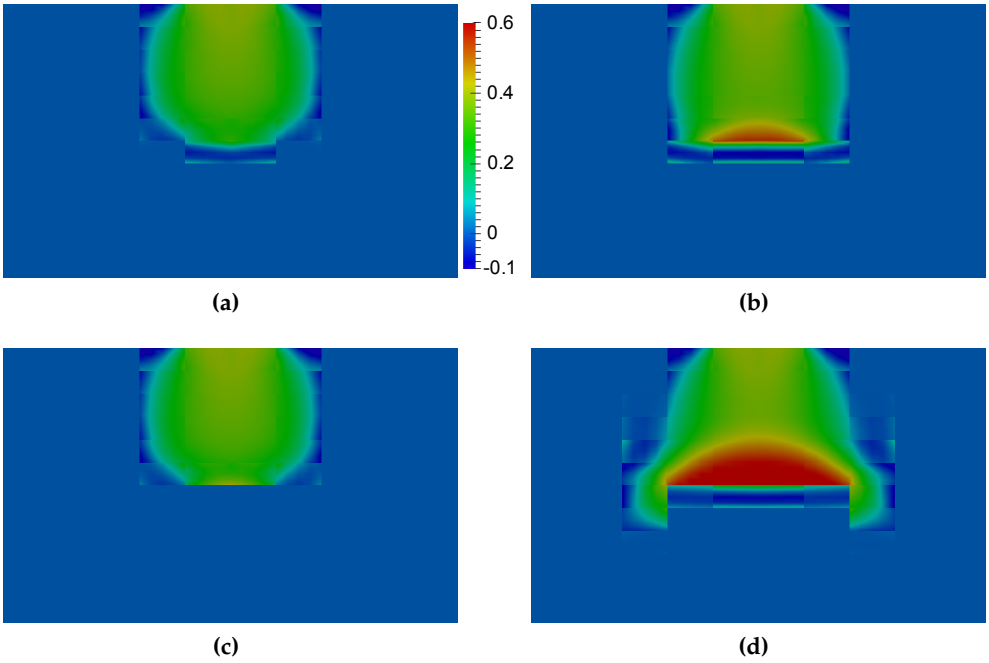

Figure 6.6: Sand lense example with discontinuous permeability and NIPG 2. order (a) at $t = 30 \cdot 35\,\mathrm{s}$ (b) last solved step at $t = 36 \cdot 35\,\mathrm{s}$ (c) with weighted averages at $t = 30 \cdot 35\,\mathrm{s}$ (d) with weighted averages at $t = 50 \cdot 35\,\mathrm{s}$

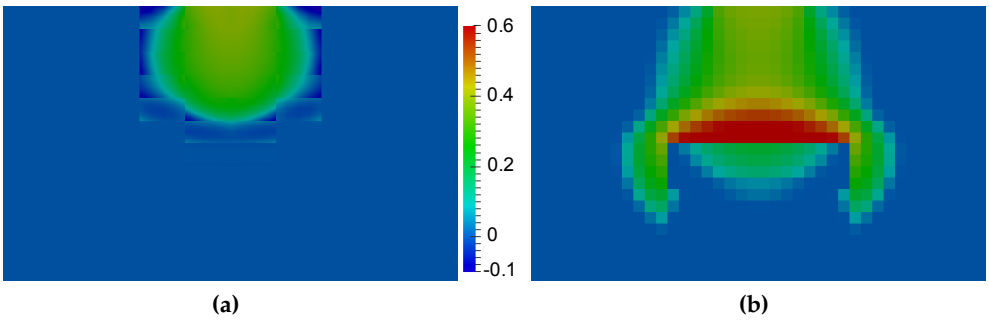

Figure 6.7: Sand lense example with fine sand lense (a) Nipg 2. order last solved step at $t = 23 \cdot 35\,\mathrm{s}$ (b) Finite volume on a 40×24 grid at $t = 60 \cdot 35\,\mathrm{s}$

is higher than the entry pressure p_{e2} of the sand lense. This results in a choking until the fluid floats around the sand lense. Later, after more non-wetting fluid has entered, the pressure becomes high enough to enter the lense.

A finite volume program in the pressure/pressure formulation exists as a PDELab example. Figure 6.5c and 6.7b are made with this program.

The DG methods do not solve this example. The choking of the non-wetting phase above the sand lense leads to a saturation jump. This results in a capillary pressure jump which becomes too high to be solved. Figure 6.7a shows the last calculated step before the Newton method does not converge anymore.

To solve this example an improvement comparable to the weighted averages would be necessary. [EMS2010] describes an approach to apply weighted average to capillary pressure jumps. This method would go beyond the scope of this work.

7 Conclusions

Discontinuous Galerkin (DG) methods are applicable to solve two-phase flows problems in porous media. The increased complexity of the implementation compared to finite element or finite volume methods can be compensated by modern software toolkits and up to date programming techniques. Some years ago a system of coupled partial differential equations including two independent variables was far too much work to be done in six months. Today this is achievable, proved by this work.

The Richards equation is flawlessly solvable with the examined DG methods. Close to steep fronts it may be necessary to treat the occurring overshots.

DG methods can solve two-phase flows examples with advantages compared to other methods. DG methods are very promising but remain very sensitive. Discontinuities can occur in the solutions but may cause problems if not treated properly.

The pressure/saturation formulation has limited applications. Many published examples contain effective saturations of 0 and 1 for one of the phases. These examples cannot be solved because the pressure of both phases would be locally undefined. The results of modified examples which match the needs of the formulation are not comparable with already published results. Artificial examples with smooth solutions can be used to demonstrate the correctness of a program or to show theoretical results. But the results cannot be transferred to real applications. A widely used and accepted set of test cases is not established. At least the Buckley-Leverett example is used in various versions in different publications.

It is evident that many details in the methods need a more exhaustive examination. In the saturation equation the capillary pressure jump is penalized. [Eps2007] uses the pressure jump of the non-wetting phase for penalization. Advantages of this choice are neither numerically nor theoretically known. The same applies to the penalty weight σ. Choosing different weights for the pressure and the saturation equation may improve the results.

Weighted averages cannot handle steep fronts in the relative permeability which is solution dependent. Indeed, a minimal amount of penalty is needed in this case, as reflected by the analysis of diffusion-convection problems with locally small diffusion. But weighted averages improve jumps in the absolute permeability significantly. In addition they are easy to implement. Averaging the capillary pressure like proposed in [EMS2010] sounds reasonable. It would be nice to generalize weighted averages to include the relative permeability.

Appendix A

Construction of the source term for the analytical example

This appendix describes how the source term q for the Richards equation test cases with analytic solutions from Chapter 5.2 can be constructed. Border conditions, initial values and the saturation function are taken from the Haverkamp example. The analytic solution (5.5) has a similar shape compared to the solutions in Figure 5.2. Besides, tangens hyperbolicus is a very smooth function so higher ordered ansatz functions will lead to better approximations.

Substituting the analytic solution into the Richards equation results in a large equation. To do the calculation only once the factor $\frac{t}{4}$ in (5.6) is multiplied with a flag $\zeta \in \{0, 1\}$ to distinguish the two test cases. The formula can be simplified to

$$q(x,t) = \begin{cases} q_u(x,t) & 408\,\tanh(\xi) + 5\,t\zeta < 822 \\ q_s(x,t) & 408\,\tanh(\xi) + 5\,t\zeta \geq 822 \end{cases} \tag{A.1}$$

with

$$\begin{aligned} q_u(x,t) = &- \frac{5247}{6250}\left|\frac{13821}{25000}\tanh(\xi) + \frac{271}{40000}\,t\zeta - \frac{111381}{100000}\right|^{\frac{74}{25}} \\ &\cdot \frac{\frac{4607}{200000} - \frac{4607}{200000}\,(\tanh(\xi))^2 + \frac{271}{40000}\,\zeta}{\left(1 + \left|\frac{13821}{25000}\tanh(\xi) + \frac{271}{40000}\,t\zeta - \frac{111381}{100000}\right|^{\frac{99}{25}}\right)^2} \\ &- \frac{13983}{312500}\left|\frac{6681}{6250}\tanh(\xi) + \frac{131}{10000}\,t\zeta - \frac{53841}{25000}\right|^{\frac{187}{50}} \\ &\cdot \frac{\left(\frac{56}{5} - \frac{51}{5}\,(\tanh(\xi))^2\right)\left(\frac{6681}{12500} - \frac{6681}{12500}\,(\tanh(\xi))^2\right)}{\left(1 + \left|\frac{6681}{6250}\tanh(\xi) + \frac{131}{10000}\,t\zeta - \frac{53841}{25000}\right|^{\frac{237}{50}}\right)^2} \\ &+ \frac{\frac{254941}{12500}\tanh(\xi)\left(1 - (\tanh(\xi))^2\right)}{\left(1 + \left|\frac{6681}{6250}\tanh(\xi) + \frac{131}{10000}\,t\zeta - \frac{53841}{25000}\right|^{\frac{237}{50}}\right)} \end{aligned} \tag{A.2}$$

and

$$q_s(x,t) = \frac{254941}{12500}\tanh(\xi)\left(1 - (\tanh(\xi))^2\right) \tag{A.3}$$

and

$$\xi = \frac{1}{2}\left(x + \frac{t}{12} - 15\right). \tag{A.4}$$

Maple 13 was used to calculate the formula and to obtain C and LaTeX sources.

Acknowledgments

This work is a milestone in terms of my education and my personal life. I would like to thank everybody who joined me walking along a part of my way. I am grateful for the received help, encouragement and solicitousness.

I spent four month in Paris at CERMICS, Écoles des Ponts ParisTech, supervised by Prof. Alexandre Ern. I would not want to miss this great experience and would like to express my deep gratitude. The same applies to Prof. Peter Bastian who made the contact with Alexandre Ern and was my second supervisor. He initiated me in numerics, partial differential equations and soil science.

Many people kindly helped me. Christian was patient with my lacking C++ skills. Felix helped me when the submission dates approached – two times. Sven thoroughly proof-read this work and gave me advises of avail. Jö, Laurent, Pablo and Steffen always answered my little but pestering questions. Kudos to the DUNE developers for providing such a powerful and complete tool.

I am glad Prof. Thomas Ertl took over my examination in Stuttgart. The secretaries in Paris, Heidelberg and Stuttgart Ms. Baccaert, Ms. Ouhanna, Ingrid and Ms. Ritzmann made me feel welcome and domestic.

The finishing touches in matters of correct English were provided by David. My brother Albert helped me with short-run cross-reading and countless consultations. My sister Miriam offered me a sleeping berth in Heidelberg whenever I needed one. I would like to thank my parents for their efforts and continuous support. With Aurelia I could share my thoughts, my problems and my spare time, thank you.

I dedicate this work to my grandfather Leopold who examined natural water resources long before I did it.

Bibliography

[ABC+2002] Arnold, Douglas; Brezzi, Franco; Cockburn, Bernardo; Marini, Donatella: *Unified Analysis of Discontinuous Galerkin Methods for Elliptic Problems*. SIAM Journal on Numerical Analysis 39.5, 1749–1779 (2002)

[Bas1999] Bastian, Peter: *Numerical Computation of Multiphase Flows in Porous Media*, Habilitationsschrift, Christian–Albrechts–Universität Kiel, 1999

[BBD+2008a] Bastian, Peter; Blatt, Markus; Dedner, Andreas; Engwer, Christian; Klöfkorn, Robert; Kornhuber, Ralf; Ohlberger, Mario; Sander, Oliver: *A Generic Grid Interface for Parallel and Adaptive Scientific Computing. Part II: Implementation and Tests in DUNE*. Computing 82.(2-3), 121–138 (2008)

[BBD+2008b] Bastian, Peter; Blatt, Markus; Dedner, Andreas; Engwer, Christian; Klöfkorn, Robert; Ohlberger, Mario; Sander, Oliver: *A Generic Grid Interface for Parallel and Adaptive Scientific Computing. Part I: Abstract Framework*. Computing 82.(2-3), 103–119 (2008)

[BHM2010] Bastian, Peter; Heimann, Felix; Marnach, Sven: *Generic Implementation of Finite Element Methods in ihe Distributed and Unified Numerics Environment (DUNE)*. Proceedings of Algorithmy 2009, to appear (2010)

[Bra2007] Braess, Dieter: *Finite Elemente*. Springer: Heidelberg, 2007

[CBZ1990] Celia, Michael; Bouloutas, Efthimios; Zarba, Rebecca: *A General Mass-Conservative Numerical Solution for the Unsaturated Flow Equation*. Water Resources Research 26, 1483–1496 (1990)

[EG2004] Ern, Alexandre; Guermond, Jean-Luc: *Theory and Practice of Finite Elements*. Applied Mathematical Sciences, vol. 159, Springer: New-York, 2004

[EMS2009] Ern, Alexandre; Mozolevski, Igor; Schuh, L.: *Accurate velocity reconstruction for Discontinuous Galerkin approximations of two-phase porous media flows*. Les Comptes Rendus Académie de Sciences Paris, Série I 347, 551–554 (2009)

[EMS2010] Ern, Alexandre; Mozolevski, Igor; Schuh, L.: *Discontinuous Galerkin approximation of two-phase flows in heterogeneous porous media with discontinuous capillary pressures*. Published in Computer Methods in Applied Mechanics and Engineering, to appear (2010)

[Eng2009] Engwer, Christian: *An Unfitted Discontinuous Galerkin Scheme for Micro-scale Simulations and Numerical Upscaling*, Ph.D. thesis, Ruprecht-Karls-Universität Heidelberg, June 2009

[Eps2007] Epshteyn, Yekaterina: *HP primal Discontinuous Galerkin Finite Element Methods for Two-phase Flow in Porous Media*, Ph.D. thesis, University of Pittsburgh, 2007

[ESZ2009] Ern, Alexandre; Stephansen, Annette; Zunino, Paolo: *A Discontinuous Galerkin method with weighted averages for advection-diffusion equations with locally small and anisotropic diffusivity*. IMA Journal of Numerical Analysis 29.2, 235–256 (2009)

[Hol1996] Holzbecher, Ekkehard: *Modellierung dynamischer Prozesse in der Hydrologie*. Springer: Heidelberg, 1996

[HVT+1977] Haverkamp, Roland; Vauclin, Michel; Touma, Jaoudat; Wierenga, Peter; Vachaud, Georges: *A Comparison of Numerical Simulation Models for One-Dimensional Infiltration*. Soil Science Society of Am. Jour. 41.2, 285–294 (1977)

[KBS+2003] Kinzelbach, Wolfgang; Bauer, Peter; Siegfried, Tobias; Brunner, Philip: *Sustainable Groundwater Management – Problems and Scientific Tools*. Episodes 26.4, 279–284 (2003)

[KL2000] Knabner, Peter; Lutz, Angermann: *Numerik partieller Differentialgleichungen*. Springer: Heidelberg, 2000

[MF2004] Manzini, Gianmarco; Ferraris, Stefano: *Mass-conservative finite volume methods on 2-D unstructured grids for the Richards' equation*. Advances in Water Resources 27, 1199–1215 (2004)

[NNa] *Wikipedia The Free Encyclopedia*, http://en.wikipedia.org, visited Feb 2010

[NNb] *Wikipedia Die freie Enzyklopädie*, http://de.wikipedia.org, visited Feb 2010

[NNc] *Dune project website*, http://dune-project.org, visited Feb 2010

[Ric1931] Richards, Lorenzo Adolph: *Capillary Conduction of Liquids through Porous Mediums*. Journal of Applied Physics 1, 318–333 (1931)

[Sch2009] Schwartz, Michael: *Modelling Groundwater Contamination above the Asse 2 medium-level Nuclear Waste Repository, Germany*. Environmental Earth Sciences 59.2, 277–286 (2009)

[Soc2008] Sochala, Pierre: *Méthodes numériques pour les écoulements souterrains et couplage avec le ruissellement*, Ph.D. thesis, Ecole des Ponts ParisTech, December 2008

[vG1980] van Genuchten, Martinus: *A Closed-form Equation for Predicting the Hydraulic Conductivity of Unsaturated Soils*. Soil Science Society of America Journal 44, 892–898 (1980)

Declaration

All the work contained within this thesis, except where otherwise acknowledged, was solely the effort of the author. At no stage was any collaboration entered into with any other party.

(Christoph Grüninger)